Spatial variability characteristics of the effective friction angle of Crag deposits and its effects on slope stability

Samzu Agbaje[1], Xue Zhang[1*], Darren Ward[2], Luisa Dhimitri[2], Edoardo Patelli[3]

[1] Department of Civil Engineering and Industrial Design, University of Liverpool, Liverpool, UK
[2]In Situ Site Investigation, East Sussex, UK
[3] Centre for Intelligent Infrastructure, University of Strathclyde, Glasgow, UK

Abstract

This study investigated the spatial variability characteristics of the effective friction angle of Crag deposits which are granular soils occur in the east of England. Cone Penetration Test data were obtained at 26 locations and interpreted statistically. The distribution characteristic of the effective friction angle of Crag deposits was derived with the mean value, the standard deviation and the correlation length calibrated. Illustrations were also shown on how factors such as ground water pressures and the existence of soft/organic soil zones affect the measurement of the autocovariance function and thus the correlation length. Bayesian inference technique was adopted alongside the method of moments to determine the correlation length. Based on the obtained statistical parameters, both semi-deterministic (based on standard geotechnical design codes) and probabilistic finite element limit analyses were carried out to investigate the stability of slopes in Crag deposits. Slopes of various inclined angles were considered and comparisons between the semi-deterministic and probabilistic results were conducted to improve the understanding of the stability of Crag slopes and to provide insight into the slope stability code used in practice.

Keywords: spatial variability; Crag deposit; slope stability; finite element limit analysis, correlation length

---

* Email: xue.zhang2@liverpool.ac.uk

This is a peer-reviewed, accepted author manuscript of the following article: Agbaje, S., Zhang, X., Ward, D., Dhimitri, L., & Patelli, E. (2022). Spatial variability characteristics of the effective friction angle of Crag deposits and its effects on slope stability. Computers and Geotechnics, 141, [104532]. https://doi.org/10.1016/j.compgeo.2021.104532

1. Introduction

Current stability analysis in practice relies heavily on the traditional total factor of safety approach in which deterministic properties of geomaterials are used in analyses without considering any uncertainties in properties (Morgenstern & Price, 1965; Baker & Garber, 1978). In the total factor of safety approach, use of the maximum strength obtained from in-situ tests overestimates the stability of a slope and leads to an unrealistic high factor of safety. The more conservative assessment of a slope can be achieved adopting the minimum strength in the stability analysis which, however, also implies the least economical solution. In earthworks, a more conservative design of a cutting slope means a much shallower and safer angle. It requires the acquisition of more land space which is costly and, in many cases, restrained by civil/legal and/or environmental/historical/cultural restrictions. Additionally, it incurs more design and construction time and resources and a higher carbon footprint. Clearly, this dilemma stems from the spatial variability and uncertainty of soil properties.

Many geotechnical design codes, such as the Eurocode 7 (British Standards International (BSI), 2004 + A1:2013), have moved from traditional total factor of safety method to the partial factor approach to account for spatial variability and uncertainty. In the partial factor approach, partial factors, which depend on variability and uncertainty, are applied to soil strength or loading. Despite its wide applications in geotechnical practice, the performance of the partial factor approach from reliability point of view is still questionable because the partial factor cannot fully cover the feature of variability and uncertainty in model parameters.

Full probabilistic analysis method is a robust technique for considering the spatial variability and uncertainty of soils in stability problems (Griffiths, et al., 2009; Jiang, et al., 2014). The realization of full probabilistic analysis involves the calibration of spatial variability of soil properties according to in-situ test, the generation of random field reflecting the variability, the implementation of the random field in numerical stability analysis method and the interpretation of simulation results. Extensive efforts have been devoted to advancing and realizing full probabilistic analysis in geotechnical engineering over the past decades. In terms of spatial variability calibration, De Groot and Baecher (1993) and Lacasse and Nadim (1996) used the method of moments and the maximum likelihood method for calculating autocovariance distance. Fenton and Griffiths (2008) provided in-depth discussions on the quantification of statistical parameters of soil properties and application to a wide range of geotechnical problems, for example groundwater modelling, deep foundations and slope stability to name a few. Cao and Wang (2013) studied probabilistic site characterization using Bayesian approach with cone penetration tests. Liu et al. (2017) presented an integrated framework, combining the restricted maximum likelihood method and the Matérn autocovariance model, for characterizing spatial variability of geological profiles. Uzielli and Mayne (2019) studied the probabilistic correlations for effective friction angle of clean to silty sands. Low (2019) investigated the probabilistic site date of soil and rock slopes from San Francisco and Hong Kong. A summary on the estimation methods for scale of fluctuation of spatially varying soils was provided by Cami et al. (2020). To generate random field, the Karhunen Loeve method is commonly used (Phoon et al., 2002; Zheng and Dai, 2017; Huang, et al., 2013) and numerical approaches which have been combined with random fields for stability problems include, but are not limited to, the limit equilibrium method (El-Ramly, et al. 2002; Jiang and Huang, 2016; Li et al. 2016; Liu et al. 2020), the finite element limit analysis method (Huang et al., 2013; Ali, et al., 2017; Krabbenhoft et al. 2018), elastoplastic finite element method (Griffiths & Fenton, 2004; Huang, et al., 2010; Dyson and Tolooiyan, 2019), Coupled Eulerian-Lagrangian method (Li et al. 2020; Chen et al., 2021). Based on these methods, influences of spatial variability on slope reliability have also been investigated to some extent for both pure cohesive and cohesive-frictional soils (Griffiths et al. 2009; Jiang et al. 2014; Jiang et al. 2015).

Despite these contributions, the application of spatial variability analysis to geotechnical problems in practice is still very limited. Indeed, the real-life scenarios are much more complex and challenge its application. For example, how a sudden change of soil type in depth (particularly the case of granular soils with organic clay layers) and severe fluctuations of pore water pressure, both of which are commonly observed in site investigation, impact the calibration of random field parameters and, consequently, slope design is yet clear and requires further investigation. Additionally, the full probabilistic analysis is computationally time-consuming which is another obstacle to its application in practice. To reduce the computational cost, semi-deterministic analysis is used that a uniform soil strength (factored or unfactored) is assigned. The failure probation of slope is then related to the likelihood of the occurrence of the specific soil strength with which the slope is stable. Although such a method does decrease the cost, its reliability is questionable given the significant simplification.

To answer these questions, we utilised Crag deposit as an example to explore the entire process of spatial variability analysis from data collection to the derivation of slope design results with emphasis on the challenges encountered due to the complexity of real scenarios. Crag deposit is found widely along the east coast of England (i.e. East Anglia) and the western margin of southern

North Sea basin. It consists of a range of marine and estuarine sands, gravels, silts and clays (Zalasiewicz, et al., 1988; Prestwich, 1871) and possesses apparent uncertainties in the spatial distribution of strength. The diverse constituents of Crag deposit pose a challenge not only to slope stability analysis therein but also the calibration of its statistical characteristics. To date, very limited data about the properties of Crag deposit have been reported. In this paper, the spatial variability of effective friction angle of Crag deposits is quantified via statistical analysis of an extensive set of self-conducted cone penetration tests (CPT) soundings. Discussions are also conducted on the influence of statistical impurities such as inclusion of organic clays in the deposit and severe changes in pore water pressure on the calibration of statistical parameters. Both full probabilistic analysis and semi-deterministic partial/total factor of safety analysis, according to standard geotechnical design code, are carried out with wide range parametric studies. Comparison between the results leads to guiding information for slope design in Crag deposit and similar geomaterials.

2. Site Investigation Survey

Owing to the intense development of critical infrastructure and industrial projects in East Anglia (e.g. Sizewell C nuclear power station and the Norwich Western Link project), many earthworks will be constructed on Crag deposits. A good understanding of Crag deposits and geostructures therein is of great importance to reduce earthwork instability risk. To this end, a survey of 26 Cone Penetration Tests (CPT) with a sampling interval of 0.01 m was carried out in an area of 85 m × 138 m in Sizewell, east coast of England, where the Crag presents with marine deposits and peat nearby (Figure 1). The Mohr-Coulomb model is adopted in light that Crag deposits are predominantly granular according to (British Geological Survey, 1996).

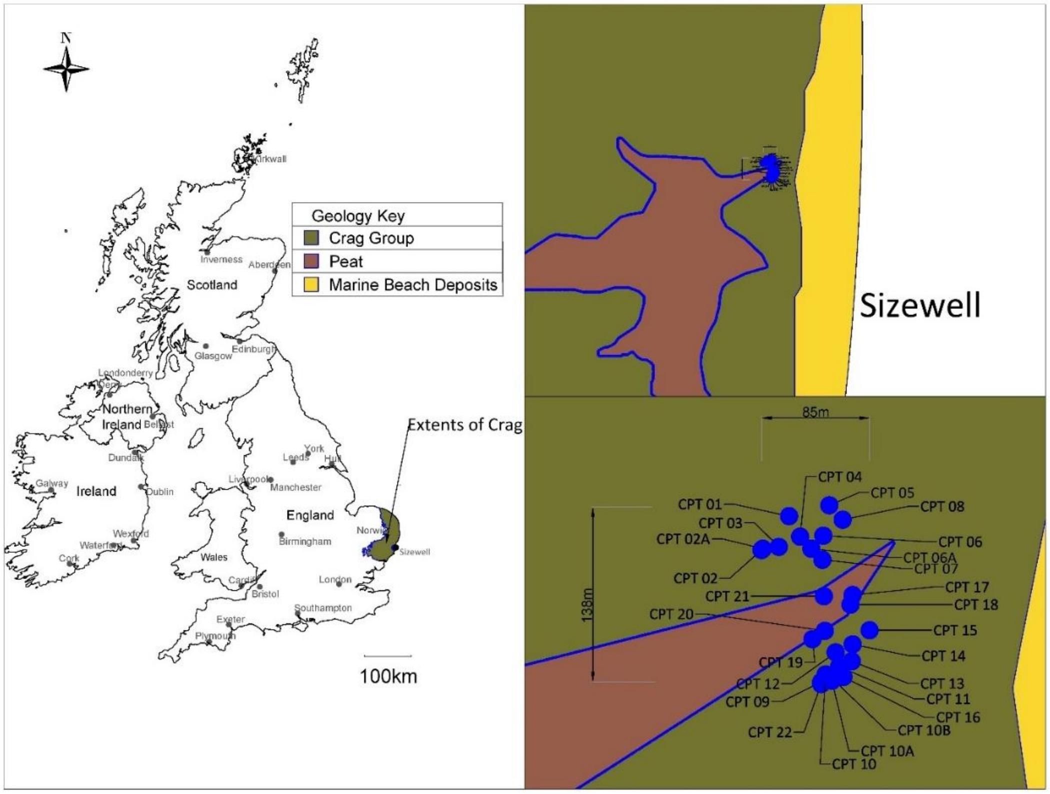

Figure 1 Crag Deposits in the East of England, UK, and the location of the site investigation survey – “Contains British Geological Survey materials” © UKRI (2021)

Up to date, there has been no universal consensus equation for calibrating effective friction angle from CPT data. Herein, the effective friction angle is calculated using the three commonly used formulations, namely

- formulation proposed by Robertson and Campanella (1983)

$$tan\,\phi' = (0.1 + 0.38\,log(\,q_t/\sigma'_{v0})) \tag{1}$$

- formulation proposed by Kulhawy and Mayne (1990)

$$\phi' = 17.6 + 11\,log[(\,q_c/p_a)/(\sigma'_{v0}/p_a)^{0.5}] \tag{2}$$

- formulation suggested in Eurocode 7 (British Standards International (BSI), 2007)

$$\phi' = 13.5\,log\,q_c + 23 \tag{3}$$

In above equations, q_t is the corrected cone resistance, q_c is the cone resistance, σ'_{v0} is the initial vertical effective stress and p_a is the atmospheric pressure. Figure *2* shows the effective friction angle calibrated using these equations for CPT 17 and CPT22. Generally, the effective friction angle calibrated using the formulation proposed by Kulhawy and Mayne (1990) is much higher than these from Robertson and Campanella (1983) and Eurocode 7. Eq. (3) suggested by Eurocode 7 is only valid for 5 MPa $\leq q_c \leq 28$ MPa and, thus, provides results for depth in a limited range (i.e. red curves in Figure *2*). However, the results from Eurocode 7 agree well with these from Robertson and Campanella (1983) which does provide a full profile. The equation from Robertson and Campanella (1983) is valid for general cases except sand of high compressibility such as carbonate sand. In the following, the effective friction angle calibrated using Eq. (1) is adopted in all analysis. The full CPT profiles are provided in Appendix for readers of interest.

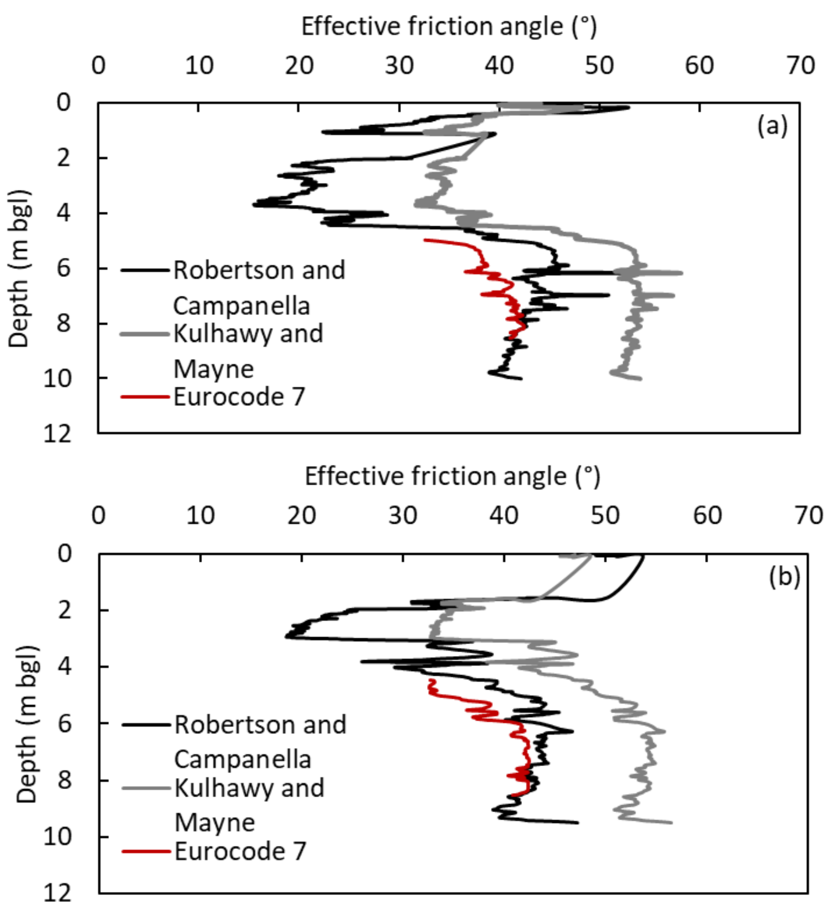

Figure 2 Effective friction angles calibrated from CPT date using different equations: (a) CPT 17 and (b) CPT 22.

The curves of effective friction angle against depth for all CPT locations are shown in Figure *3*. For depth ≤ 4 m, an apparent variation of ϕ' is observed. The range of variation is from 13.8° to 64.2° and decreases with depth. For example, the effective friction angle varies between 27° and 52° at the depth of 7 m and between 38° and 45° at the depth of 10 m. It is also indicated that the final depths the penetrometer reached at most CPT locations are in between 7.33 m and 12.02 m. Tests of CPT 09 and CPT 16 terminated at the depth less than 1 m due to a refusal on tip resistance which is caused by the obstruction from large gravels/cobbles.

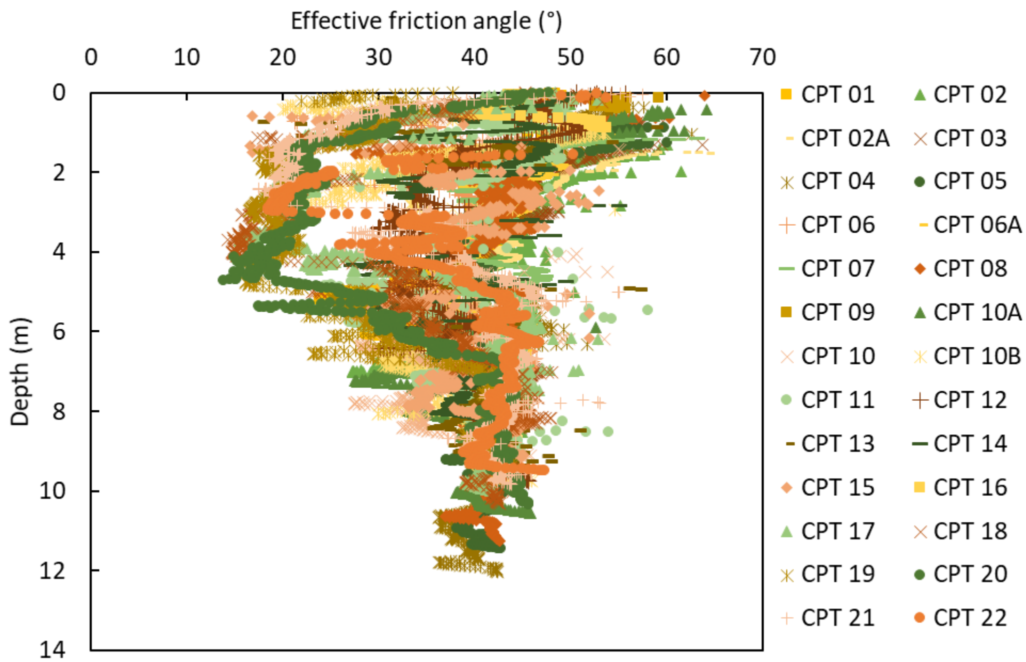

Figure 3 Effective friction angle obtained from 26 CPT tests

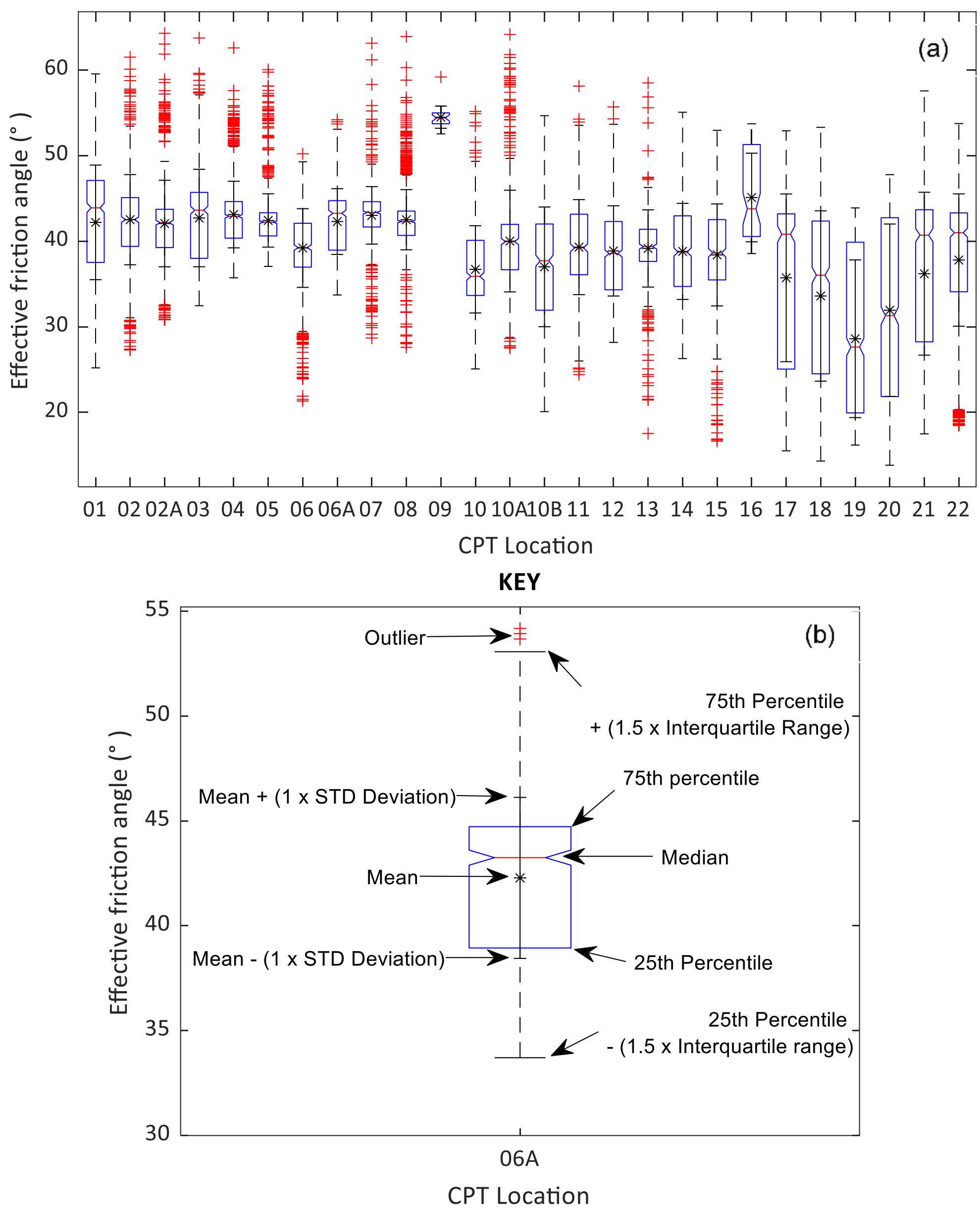

Figure 4 CPT survey data per location: (a) boxplots of data (b) key to boxplots

Figure *4* shows the statistical results of the effective friction angle, ϕ', per CPT location. A wide range of ϕ', between the 25th and 75th percentiles indicating a change of 15° to 20°, is observed for CPT series from 17 to 21. This can be explained by the fact that locations of CPT 17 to CPT 21 are very close to peat as shown in Figure *1*, suggesting that the presence of organic content results in a considerable standard deviation of ϕ'. These locations also owe relatively lower mean value of ϕ' because of the presence of peat. On the contrary, all other locations have a narrow range of ϕ' between the 25th and 75th percentile - typically a change less than 10°. Very few data are obtained from CPT 09 because the presence of large gravels and cobbles made it terminate at a very early stage with the final reached depth being 0.4 m. The mean of ϕ' for CPT 09 is thus much higher than others as shown in Figure *4*(a).

3. Mean and standard deviation of effective friction angle

A total of 19,045 values of the effective friction angle, ϕ', are obtained from the CPT tests. To further investigate the spatial variability of the strength. The mean and standard deviation of ϕ'were calculated in two ways. In option A, we assume that ϕ' across the soil domain obeys the same spatial distribution, and thus all values of ϕ' were treated as from a single sample and adopted to determine the mean and the standard deviation for the soil domain. In option B, we assume the spatial variability characteristics might be different at different depth and, consequently, the mean and the standard deviation of ϕ' at different depths are determined. This is achieved by first dividing soils into layers with specific intervals and then the statistical characteristics are calibrated using the values of effective friction angle associated with the layer.

3.1 Statistical option A

In this section, soils across Crag deposit are assumed to obey the same spatial variability characteristic. Hence, a sample consisting of all 19,045 values was used to determine the statistic distribution of ϕ'. The frequency and Cumulative Distribution Function (CDF) of ϕ' are illustrated in Figure 5. It was obtained via sorting the values of ϕ' in an increasing order followed by undertaking a count of ϕ'. Both the ideal normal and log-normal distributions were drawn for comparison. The illustrated cumulative distribution function of the normal distribution is with the mean value $\mu_{\phi'} = 38.79°$ and the standard deviation $\sigma_{\phi'} = 7.86°$ estimated based on the samples. Given that the random variable is lognormally distributed if the natural logarithm of the random variable obeys normal distribution, the CDF of log-normal distribution in Figure 5(b) is with $\mu_{ln(\phi')} = 3.63°$ and $\sigma_{ln(\phi')} = 0.239°$ which are the mean value and the standard deviation of the natural logarithm of variable ϕ' (i.e. $ln\,\phi'$), respectively.

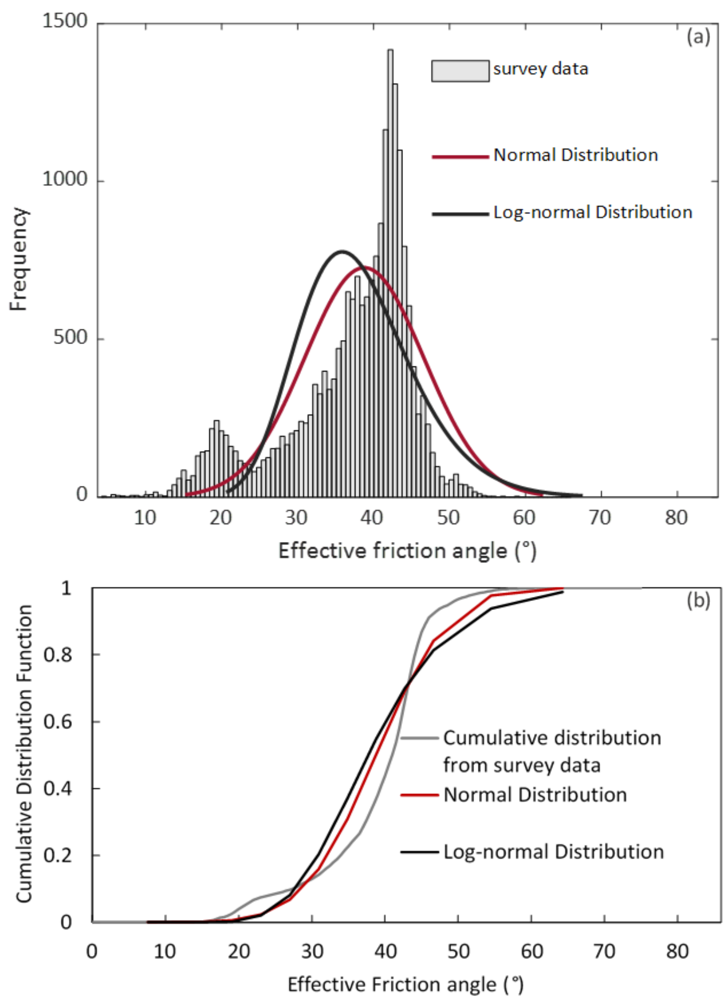

Figure 5 (a) Frequency and (b) Cumulative Probability Distribution of Crag deposit (option A)

Both the normal and log-normal distributions are very close in terms of representing the distribution of ϕ' as shown in Figure 5. The normal distribution curve has a skewness value of +1 and a kurtosis value of -1 and the log-normal distribution curve has a skewness value of +2.7 and a kurtosis value of -1.7 with the skewness and kurtosis being defined as

$$\text{*Skewness} = \frac{1}{N}\sum_{i=1}^{n}\left[\frac{\phi'_i-\mu_{\phi'}}{\sigma_{\phi'}}\right]^3 \quad (3)$$

$$\text{*Kurtosis} = \frac{1}{N}\sum_{i=1}^{n}\left[\frac{\phi'_i-\mu_{\phi'}}{\sigma_{\phi'}}\right]^4 \quad (4)$$

For the log normal distribution skewness and kurtosis, ϕ', $\mu_{\phi'}$ and $\sigma_{\phi'}$ in Eqs. (3) and (4) should be replaced by $\ln\phi'$, $\mu_{ln(\phi')}$ and $\sigma_{ln(\phi')}$, respectively. Since the normal distribution curve possesses smaller absolute values of skewness and kurtosis, it is concluded that the effective friction angle of Crag deposits more likely obeys a normal distribution rather than a log-normal distribution.

3.2 Statistical option B

The data was further analysed by calculating the mean and standard deviation of the effective friction angle against depth. This was conducted by dividing the Crag deposit into layers with a specific thickness interval. The mean and standard deviation of ϕ' at each interval are then determined using the survey data associated with the interval. Figure 6 shows the results with sampling intervals being 0.1 m, 0.5 m, 2 m and 4 m, respectively. The trends of the mean and standard deviation of effective friction angle against depth for all cases are similar despite that the curve is more fluctuated when the interval is small. Based on the variation of statistical parameters against depth, the Crag deposit can be divided into three statistical zones:

(1) Zone I – 0 m to 3 m below ground level (bgl)

The mean of effective friction angle experiences an overall decrease from 47° to 34.5° with the presence of fluctuation. The standard deviation in Zone I is much higher than those from other zones - between 7.0° and 12.0°. The high deviation from the mean value is most likely due to the existence of organic content, which leads to ϕ' lower than the mean, and to the compaction from human or environmental effects which leads to ϕ' higher than the mean.

(2) Zone II – 3 m to 9 m bgl

This is a transition zone between Zone I and Zone III. In this zone, the mean of ϕ' increases gradually from 34.5° to 42° and the standard deviation reduces gradually from 10.0° to 2.0°.

(3) Zone III – 9 m to 12 m bgl

The mean of ϕ' fluctuates somewhat around 41.6°, and the standard deviation is very small (i.e. less than 2.5°).

For simplification, we divided the 19,045 sampling points into three sub-samples based on the zones identified in Figure 6. Regarded as Option B, the mean and standard deviation are assumed uniform across each zone and calculated based on the specific sub-sample. For Option B, the mean values for Zones I and II are very similar, namely $\mu_{\phi'} = 38.51°,\ 38.63°$, respectively, and close to that from Option A (i.e. $38.79°$). The mean for Zone III is somewhat higher (i.e. $41.60°$). On contrary, there is a clear decrease in the standard deviation for Option B, namely $\sigma_{\phi'} =$

10.84°, 6.53° and 1.84° for Zones I, II and III, respectively. A comparison between the statistical characteristics between Options A and B are shown in Figure *7* reflecting these observations.

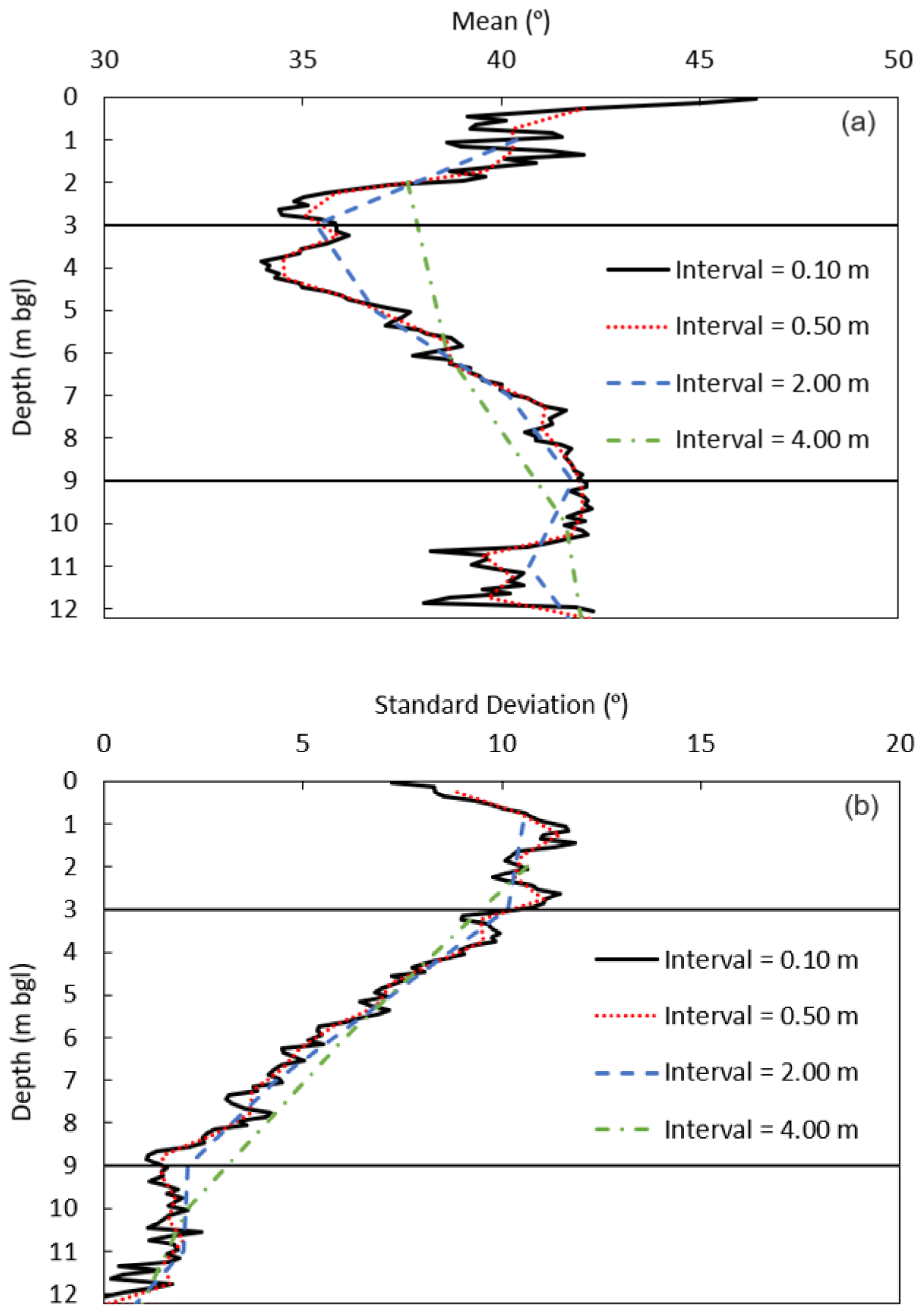

Figure 6 Variation of statistical properties of Crag deposits against depth: (a) mean and (b) standard deviation of effective friction angle determined with layer thickness interval being 0.1 m, 0.5 m, 2.0 m and 4.0 m.

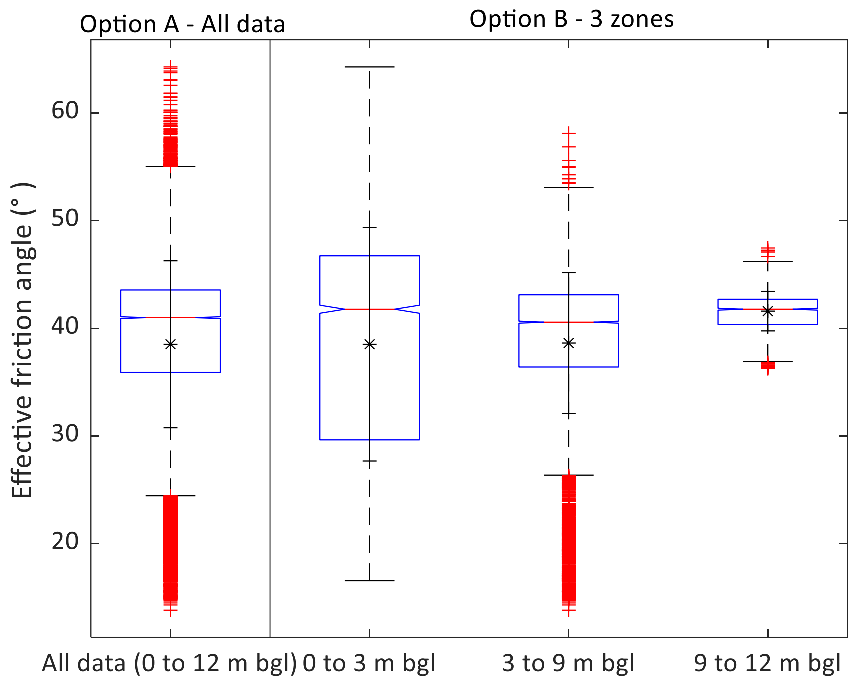

Figure 7 CPT survey data for Option A and Option B

4. Correlation length

The Correlation Length (CL), sometimes referred to as the scale of fluctuation (Fenton & Griffiths, 2008), is a characteristic length describing the extent of spatial correlation. The method of moments (De Groot & Baecher, 1993) is normally used to estimate the CL. In the method, an autocovariance function is defined

$$\hat{C}(r_j) = \frac{1}{n}\sum_{i=1}^{n-j+1}(Y_i - m_y)(Y_{i+j-1} - m_y), \quad j = 1,2,\ldots,n \tag{5}$$

where $r_j = (j-1)\Delta z$ is the lag with Δz being the distance between two points, Y_i is the soil property at point i and $m_y = \frac{1}{n}\sum Y_i$ is the sample average of Y_i. The CL is then the area under the correlation function (Vanmarke, 1983)

$$\rho(r_j) = \frac{\hat{C}(r_j)}{\hat{C}(0)} \tag{6}$$

where $\hat{C}(0)$ is the autocovariance function for $r_j = 0$. As the value of Y_i or Y_{i+j-1} tends to m_y, the autocovariance function $\hat{C}(\mathrm{r_j})$ approximates null implying a minimum deviation of the data from the mean.

In the method of moments, CL is assumed a deterministic unknown constant implying that surveying data from each CPT location results in one single CL. The values of vertical estimated using the method of moments for all CPT soundings are shown in Figure 8. For Option A, the CL ranges from 0.01 m to 0.57 m with a 50% percentile being 0.08 m. For option B, the CL for the three zones varies from 0.01m to 0.28 m, 0 to 1.21 m, and 0 to 0.19 m with corresponding 50% percentiles being 0.05 m, 0.09 m and 0.05 m, respectively.

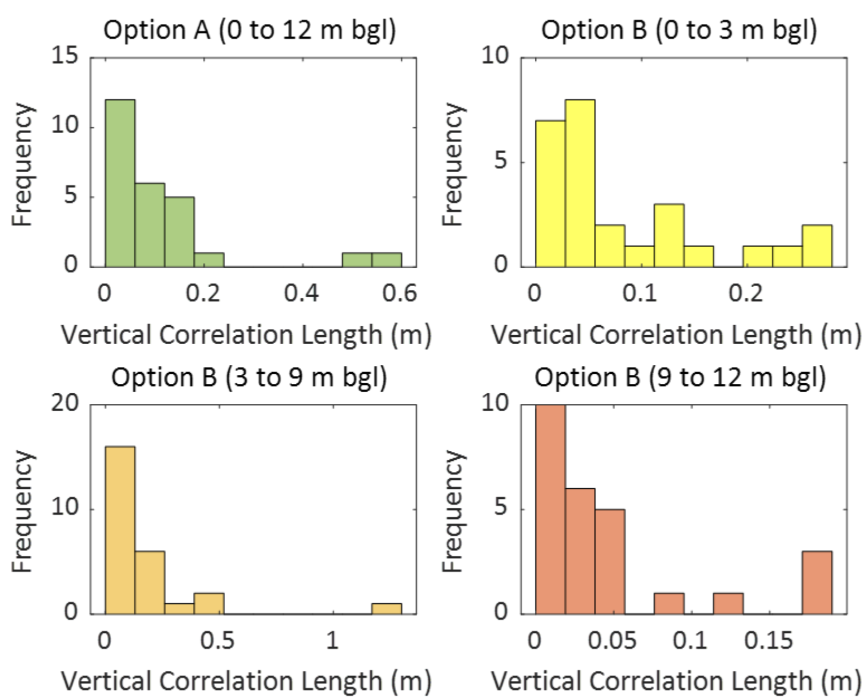

Figure 8 Frequency of vertical correlation length obtained in options A and B

Notably, the above-mentioned conventional method of moments might be of less precision for CL estimation (Cami, et al., 2020). This is because, in autocovariance function fitting, the data has to be adapted to a mathematical model such as the markov and gaussian models (Vanmarke, 1983)

$$\rho(r_j) = e^{-}\left(\left|{}^{Ar_j}/_{r_0}\right|\right)^{B} \tag{7}$$

where A is a model constant per CPT location, r_j is as defined in equation 5, r_0 is the correlation length, B equals 1 and 2 for markov model and gaussian model, respectively. The fitting, in some cases, is not able to reflect the variations of autocovariance function well, particularly when there is a sudden change in soil types or severe variation in pore water pressure which are very common in practical scenarios. In the following, some typical observations about the nature of the decay of autocovariance functions in our studies are presented and discussed.

Observation 1:

The autocovariance function decays quickly but with small, rare spikes (Figure *9*).

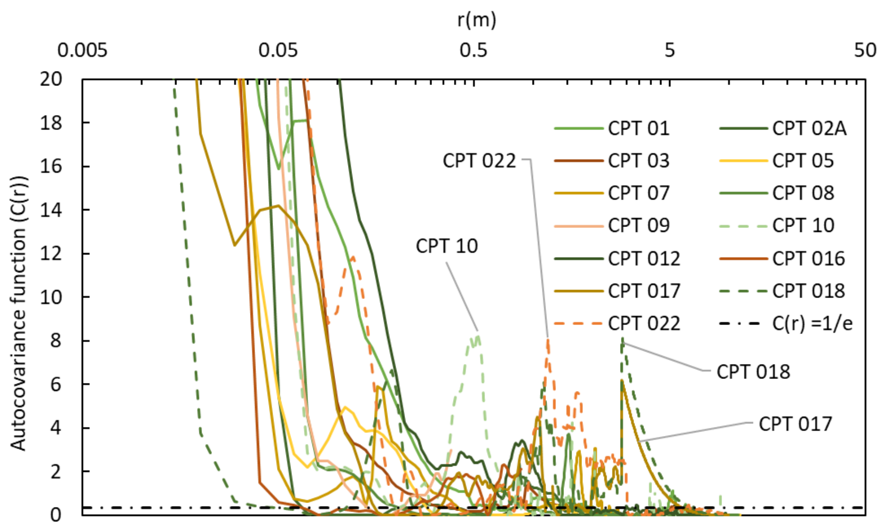

Figure 9 A fast decay of autocovariance function followed by spikes

To investigate the cause of the small spikes in autocovariance function, the Soil Behaviour Type index (SBT) based on (Robertson, 2010) was calculated. The charts of the SBT for CPT 10, CPT 17, CPT 18 and CPT 22 (Figure *10*(b) and (c)) for which spikes were observed are compared with that for other CPT tests (Figure *10*(a)). As shown, the locations of the small spikes (e.g. CPT 10 at 0.5 m bgl, CPT 17 and CPT 18 at 3 m bgl and CPT 22 at 1.2 m bgl) coincide with the depths at which a sudden change to a much softer soil, for example organic clay (SBT =2), occurs. It is thus concluded that the change to softer soils leads to the small spikes in autocovariance function for Crag deposit.

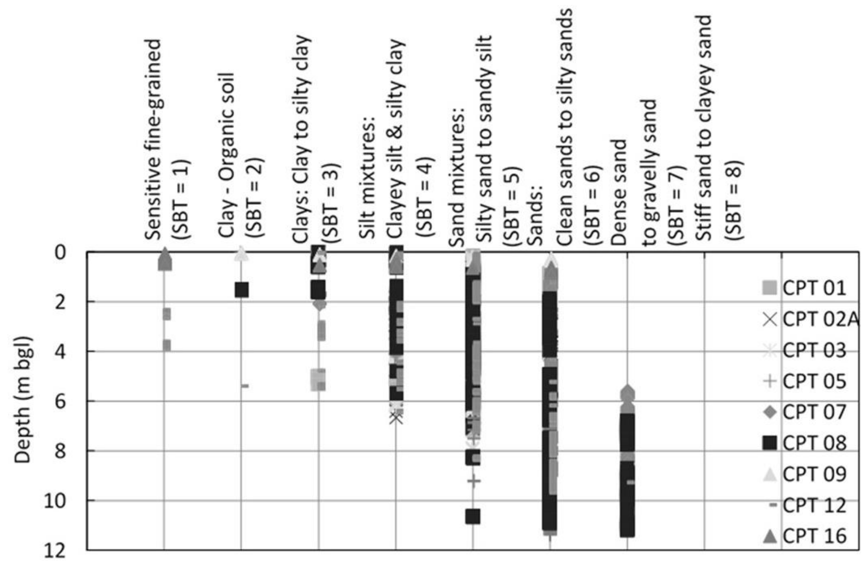
Sensitive fine-grained (SBT = 1)
Clay - Organic soil (SBT = 2)
Clays: Clay to silty clay (SBT = 3)
Silt mixtures: Clayey silt & silty clay (SBT = 4)
Sand mixtures: Silty sand to sandy silt (SBT = 5)
Sands: Clean sands to silty sands (SBT = 6)
Dense sand to gravelly sand (SBT = 7)
Stiff sand to clayey sand (SBT = 8)
Depth (m bgl)
0
2
4
6
8
10
12
CPT 01
CPT 02A
CPT 03
CPT 05
CPT 07
CPT 08
CPT 09
CPT 12
CPT 16

(a)

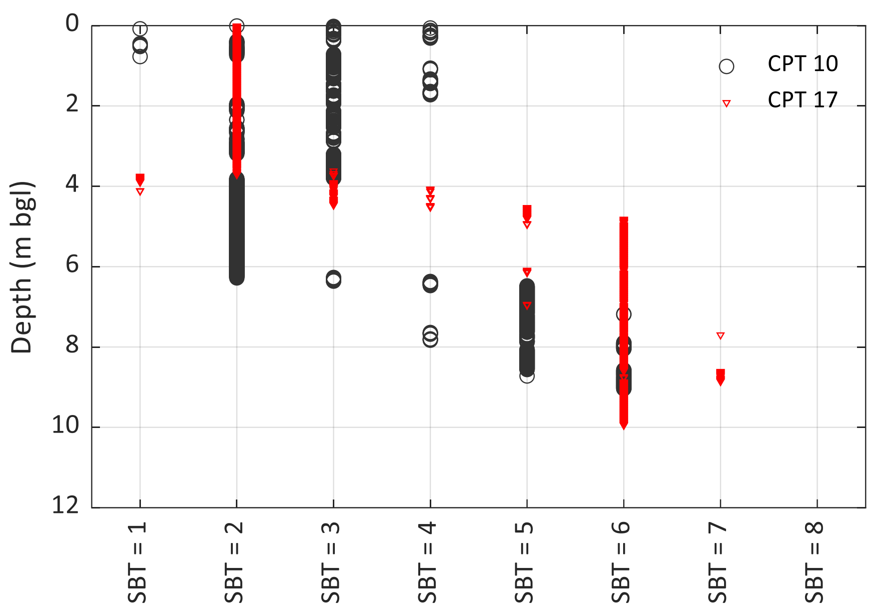
Depth (m bgl)
0
2
4
6
8
10
12
CPT 10
CPT 17
SBT = 1
SBT = 2
SBT = 3
SBT = 4
SBT = 5
SBT = 6
SBT = 7
SBT = 8

(b)

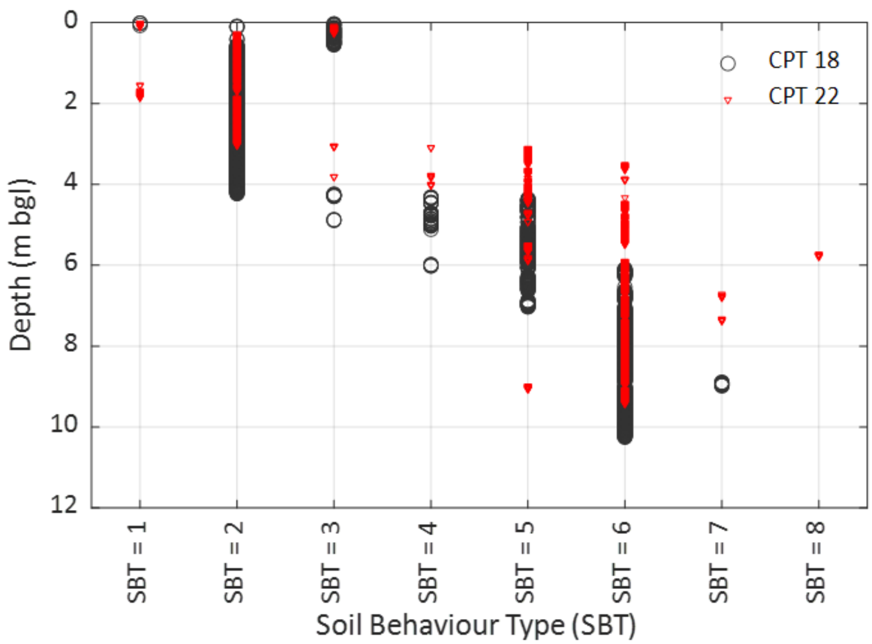

(c)

Figure 10 The chart of SBT for CPT locations (a) without organic soils (ISBT=2) soils and with organic soils at (b) CPT 10 and 17 and (c) CPT 18 and 22

Observation 2:

The autocovariance function contains frequent large spikes (Figure *11*).

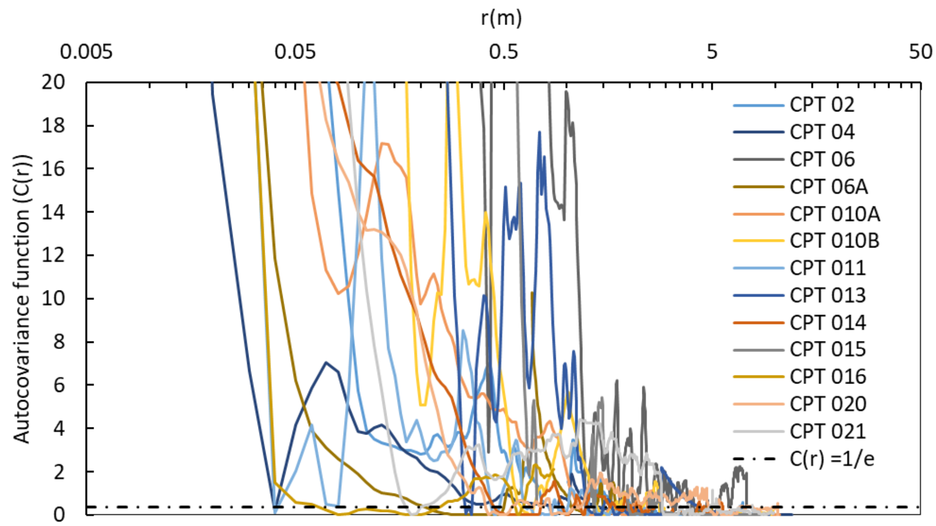

Figure 11 Decay of autocovariance function with frequent large spikes

It is deemed that these frequent large spikes result from severe oscillation of in-situ ground water pressure. Such oscillation is also associated with the clayey area. For demonstration, a comparison between the pore water pressure profiles between CPT locations without frequent large spikes and locations with large spikes is shown in Figure *12*. As shown, all these CPT locations with severe oscillation in pore water pressure have frequent large spikes in autovariance function.

For both sets of pore water pressure profiles (with or without spikes), some CPT locations showed a reduction of ground water pressure with depth. This suction (loss of water pressure) and sudden spikes phenomenon are considered typical natural features of Crag Deposits. Indeed, a review of historical borehole logs on the Geology Viewer (British Geological Survey, 2021) shows that Cable Percussive (CP) boreholes frequently encounter blowing, manifested as a sudden rise in soil within the CP borehole casings due to pore water pressure changes, when drilling at locations with Crag.

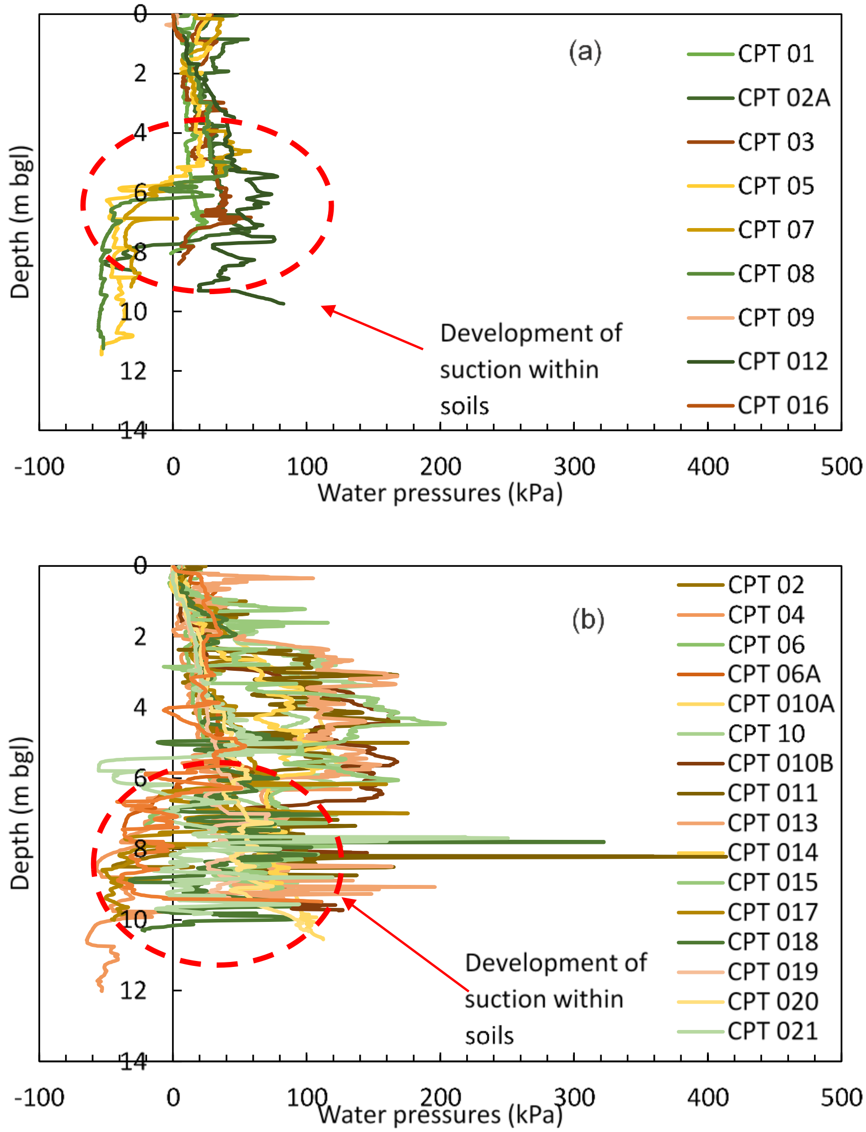

Figure 12 Pore water pressure profiles from CPT tests for cases of autocovariance function (a) without frequent large spikes and (b) with large spikes

Although the above two observations are for Option A. Similar phenomena have been observed for Option B. These observations show that certain in-situ features significantly affect soil variability.

To provide a more rigorous estimation of the CL, Bayesian inference in conjunction with the method of moments can be used (Cami, et al., 2020). The Bayesian analysis assumes that the scale of fluctuation is a possibly related random variable rather than a constant so that the statistical uncertainty is automatically included. The use of such Bayesian inference techniques to calculate CL has been discussed in (Cami, et al., 2020) and (Ching, et al., 2018). In this study, the Bayesian inference model proposed in (Lye, et al., 2021b) is adopted and the resulting autocovariance function for CPT 013 is shown in Figure 13. As illustrated, the range of posterior curves are obtained for the autocovariance function using the Bayesian inference model. The CL (value of the autocovariance Function at 1/e) is thus obtained as a range of values between the maximum CL (i.e. the vertical red dash line) and the minimum CL (i.e. the vertical black dash line) per CPT location, which also covers the value of CL from the conventional method of moments. A summary of the CL determined from the Bayesian inference model is shown in Table 1. To investigate the effect of the CL on the slope design in Crag deposit, parametric studies are carried out in the numerical simulation. The worst-case correlation length (Cami, et al., 2020; Malekpoor, et al., 2020), which results in the highest probability of failure, is also sought out.

The above discussion is for the estimation of vertical correlation length. The calibration of horizontal correlation length can be achieved using the same method; however, the CPT separation distance should satisfy specific criterions. DeGroot and Baecher (1993) concluded that the CPT separation distance should be less than the actual scale of fluctuation so that the horizontal correlation length can be calibrated properly. Ching et al. (2018) proposed a new method for estimating the horizontal correlation length in which the CPT separation distance should be less than twice of the horizontal correlation distance. The horizontal correlation length is normally much larger than the vertical correlation length and its influence is less. Thus, in this study the effect of horizontal correlation length is not considered.

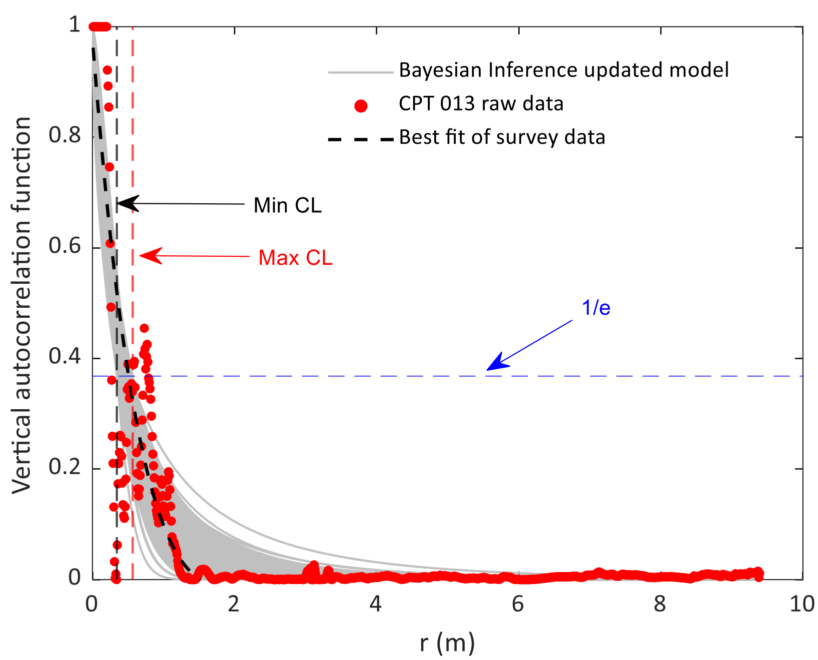

Figure 13 Decay of autocorrelation function from the conventional method of moments and the Bayesian inference model for CPT 13

Table 1 Range of the correlation length (CL) obtained from the Bayesian inference model

	Option A (0 to 12 m bgl)	**Option B** (0 to 3 m bgl)	**Option B** (3 to 9 m bgl)	**Option B** (9 to 12 m bgl)
Minimum CL (m)	0.01	0.01	0.01	0.01
Maximum CL (m)	0.60	0.61	4.21	0.31

5. Slope stability analysis

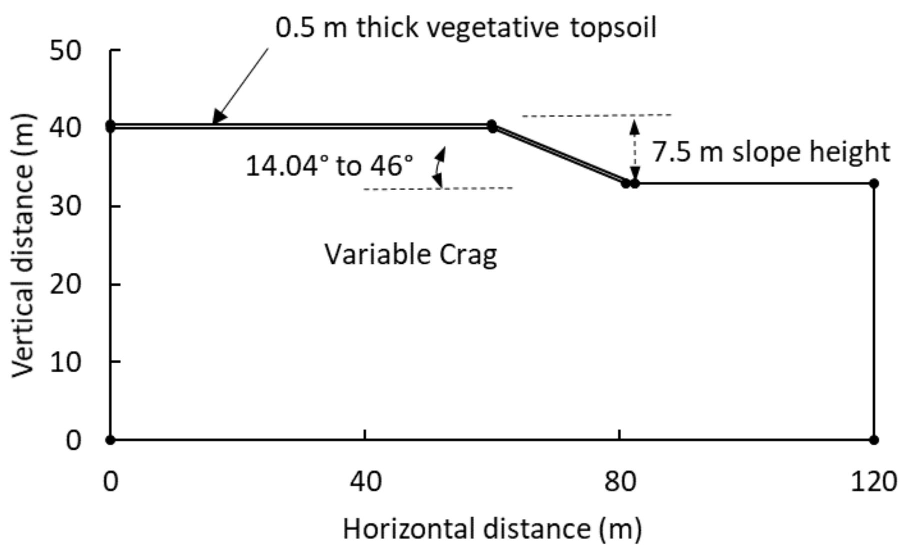

Figure 14 - Probabilistic slope stability design model

Slopes are utilised in the Geotech projects in East Anglia and a study has been undertaken to measure the cause and effect of variability and thus the risk involved in slope construction on Crag. The design model is illustrated in Figure *14* and the analyses were undertaken using a single random variable approach with the finite element limit analysis available in OptumG2 software package to calculate the Probability of Failure (PF) (Melchers, 1987). In lower bound (LB) finite element limit analysis, collapse will not occur if any state of stress can be found which satisfies the equations of equilibrium, the boundary conditions on stress and for which the yield criterion is not violated, for instance the loads are not greater than the actual collapse loads (Drucker & Prager, 1952). In upper bound (UB) finite element limit analysis, collapse occurs if for any compatible flow pattern, considered as plastic only, the rate at which work on the body due to external forces equals or exceeds the rate of internal dissipation.

The single random variable approach as shown in (Griffiths & Lane, 1999) involves analyses defining a shear strength parameter, for example ϕ' in this study, as a probability distribution function. The utilised finite element limit analysis is equipped with mesh adaptive techniques and random field generation. The slopes concerned are under the following assumptions:

- Slopes are of a geometry such that plane strain conditions apply.
- Adequate drainage is provided within slopes to ensure fully drained conditions.
- A thin layer (0.5 m) of vegetated topsoil is included in the model, with unvaried values for clarity, to mitigate against surface erosion and shallow slip surfaces. The drained cohesion c' of the topsoil is 5 kPa which is within the range of root cohesion (4 kPa – 12 kPa) as reported in (Liang, et al., 2015). The effective friction angle ϕ' of the top soil is 42° which is the global average value of effective friction angle of the top 0.5 m from our CPT data. The material properties of the topsoil are not treated as random fields.
- The horizontal correlation length (CL) is assumed sufficiently large so that it does not have influence on the probabilistic analysis of the slope stability.
- This study adopts the single random variable approach for ϕ', so the unit weight has been assumed to not vary spatially and is equivalent to a uniform value of 20 kN/m^3 which is a typical value given in BS 8002 (British Standards International (BSI), 2015). The effective

cohesion of Crag in this study is null according to BS 8002 (British Standards International (BSI), 2015) that the cohesion parameter (c') should be taken as zero in the absence of specific testing.

- The effective friction angle is assumed to obey normal distribution in the probabilistic analysis according to the statistical analysis of the survey data.

6. Simulations and discussions

In this section, semi-deterministic and full probabilistic analyses were carried out with simulation results being compared.

6.1. Semi-deterministic analyses

In semi-deterministic analysis, no uncertainty or spatial variability of ϕ' exists implying a uniform value of ϕ' across the soil domain. Two sets of semi-deterministic analyses are performed: unfactored analysis and analysis with Eurocode 7 – Design Action 1, Combination 2 (DA1 C2). In analysis with Eurocode 7 (DA1 C2), a partial factor was applied to the effective friction angle (i.e. the value of tan ϕ' was reduced to 0.8tan ϕ').

To understand the influence of ϕ', the uniform value of ϕ' across the soil domain was varied from 15.21° to 62.37° corresponding to ϕ'mean (38.79° based on Option A in Figure 4) ± 3×standard deviations, where 1 standard deviation = 7.86° in Option A. The analysis was carried out for slopes with angle varying from 14.04° to 46° which are the typical slope angles constructed in projects at East Anglia. A summary of the results for the FoS versus ϕ' versus slope angle is presented in Figure 15 (a) and (b) where the maximum value of the Factor of Safety (FoS) was 1.0. The semi-deterministic Cumulative Distribution Function (CDF) in Figure 15(c) and (d) for each set of analyses was inferred from the CDF of occurrence of ϕ' in the slope (based on the normal distribution from the survey data from Figure 5). For instance, for every slope analysed the FoS is plotted versus the cumulative likelihood of occurrence of the value of ϕ' utilised (based on the normal distribution from the survey data from Figure 5). The PF is thus defined as the CDF when the FoS is equal to 1.0. The PF versus slope angle and ϕ' is shown in Figure 15(e) and (f).

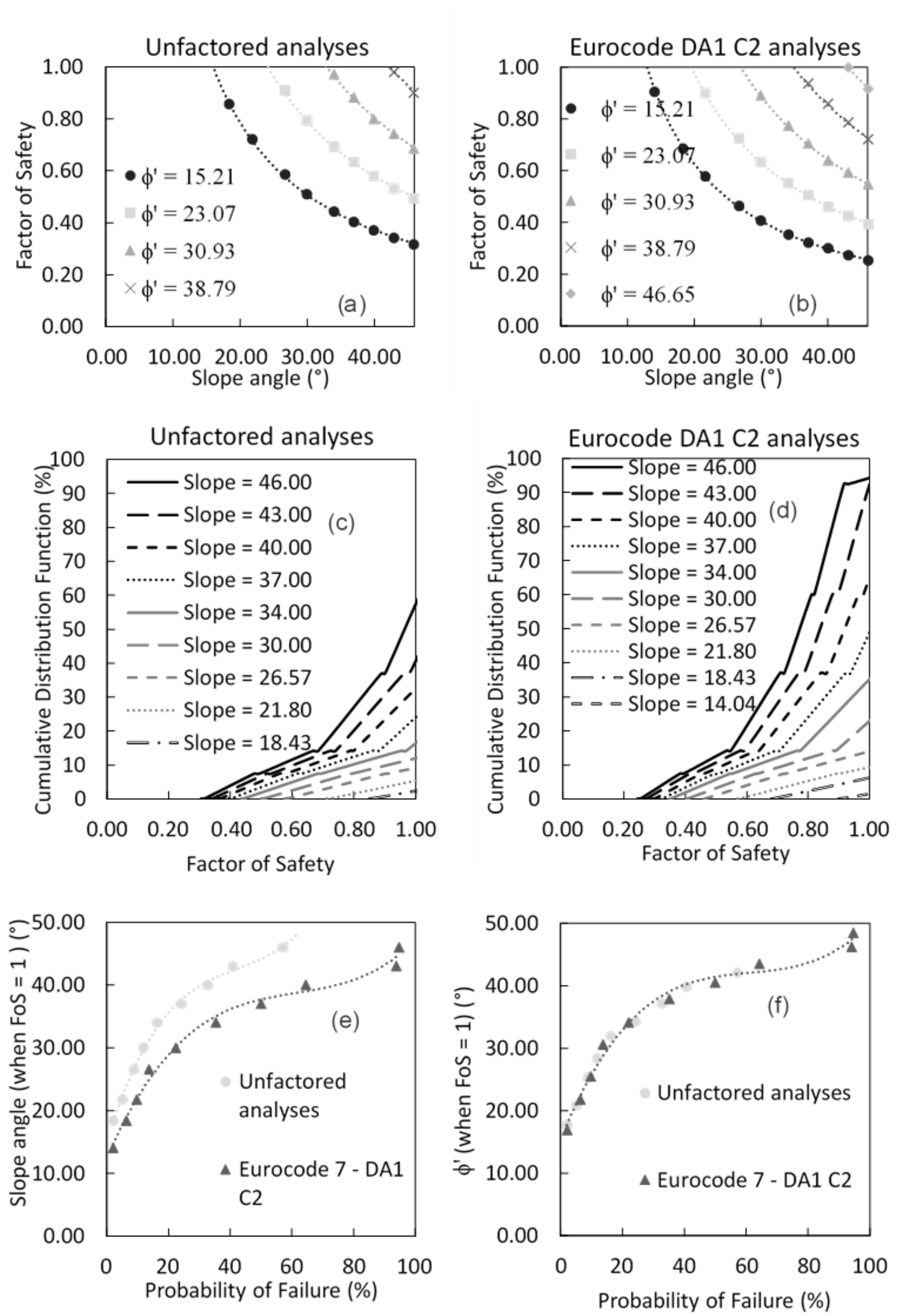

Figure 15 - Probability of Failure based on semi-deterministic analyses

Figure 15 (e) shows that a PF of 0% would be achieved in Crag for a slope of 18.43° (1 in 3 slope) for unfactored analyses and 14.04° (1 in 4 slope) for Eurocode analyses. For the mean effective friction angle ϕ'_{mean} (i.e. 38.79°), a PF of 41% (slope at failure = 43°) would be obtained for an unfactored analyses whereas the same slope angle at failure using Eurocode would predict a PF of 94%. To investigate the effects of these margin of safety provided by the partial factor (Eurocode) approach, the results of these semi-deterministic analyses are compared to those from full probabilistic analyses in the next section.

6.2. Probabilistic Analyses

The main difference between the semi-deterministic and the probabilistic approach is that the probabilistic analyses considered explicitly the spatial variation of ϕ'. The statistics (mean and standard deviation) utilised for the probabilistic analyses are based on those estimated as shown in Figure 5 while parametric studies were undertaken for the correlation length as it was shown to be probabilistic in nature. For Option A, as presented earlier, the mean value is $\mu_{\phi'} = 38.79°$ and the standard deviation is $\sigma_{\phi'} = 7.86°$. The spatial variation/random field modelling was generated based on the Karhunen-Loeve (KL) expansion method. This method creates a realisation of spatially variable random fields of the parameter (ϕ') based on an expansion of the autocovariance function using eigenvalues and eigen functions based on Mercer's theorem. A review of the KL expansion for random field generation is described in (Abrahamsen, 1997; Phoon, et al., 2002; Huang, et al., 2013; Jiang, et al. 2015). As the CL of Crag deposit varies per CPT location. It is important to understand its effects on the FoS and PF. Thus, parametric studies were also carried out with a wide range of the CL from 0.05m to 50m which covers the calibrated range of CL from the CPT data.

Probabilistic analysis of 28 cases were conducted using the finite element upper/lower bound limit. The total number of simulations (N_{sim}) per calculation for probabilistic analyses was 1000. Figure 16 shows the variation of the mean value and the standard deviation of the FoS against the number of simulations. When the simulation number is small (i.e. less than 100 simulations), the mean FoS varies between 1.004 and 1.039 (a divergence of approximately 3.5%). However, as the number of simulations increases, the mean FoS converges to 1.024 which corresponds to the 50th percentile (Median) FoS for 1000 runs. The maximum divergence of the mean FoS when over 500 simulations is less than 0.1%. Similarly, when the sample size is less than 100, the standard deviation of the FoS is up to 0.04. However, for over 500 simulations the standard deviation of the FoS is typically less than 0.005, tending towards a value of 0.002.

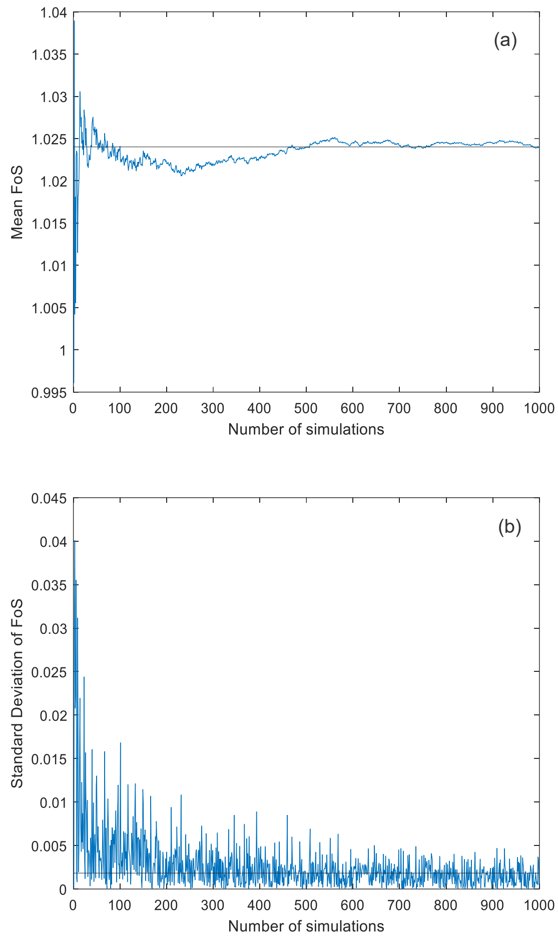

Figure 16 - Verification of number of simulations

Table 2 - Probability of Failure for various slope angles and correlation length (CL). Probability of failure with grey background indicate the case that slope angle is less than ϕ'_{mean} and CL is within the calibrated range from CPT data. UB and LB represent results from upper bound and lower bound limit analyses, respectively.

Slope angle (°) / **CL (m)**	14.04	30	34	37	40	43	46
0.05 (UB)	0%	0%	0%	7%	74%	100%	100%
0.05 (LB)	0%	0%	0%	0%	23%	91%	100%
0.5 (UB)	0%	2%	11%	29%	57%	84%	96%
0.5 (LB)	0%	1%	7%	21%	46%	76%	93%

5 (UB)	0%	10%	21%	32%	48%	63%	77%
5 (LB)	0%	8%	19%	31%	44%	60%	73%
50 (UB)	0%	10%	22%	34%	45%	58%	71%
50 (LB)	0%	9%	20%	31%	42%	56%	71%

Table 2 shows the probability of failure for all 28 cases from upper bound and lower bound finite element limit analysis. It was observed that at slope angles less than a value close to the global mean ϕ'_{mean} (in this instance 37°), the PF increases as the correlation length was increased. On the contrary, for slopes at angles greater than the global mean ϕ'_{mean} (in this instance ≥43°), the PF decreases as the correlation length increase. There appears to be a transition zone (in this instance between 37° and 43°) in between. When CL is greater than 5 m, its influence on the PF is very small.

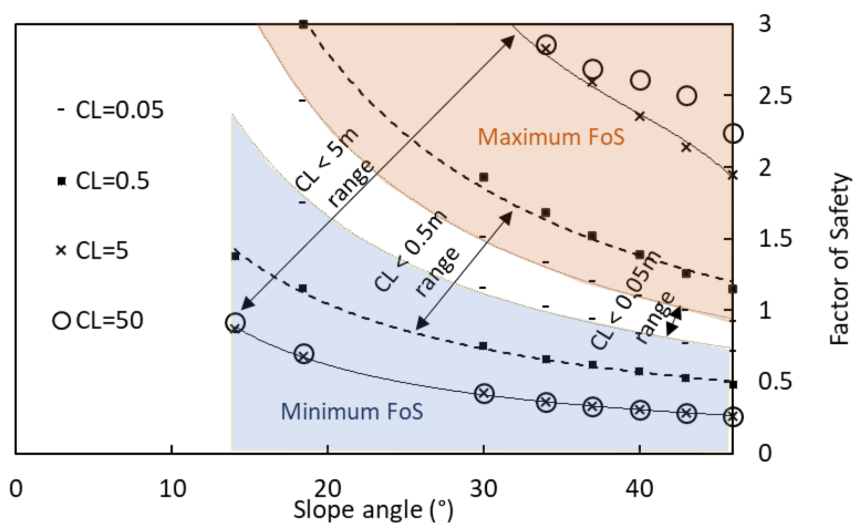

Figure 17 The range of FoS from the probabilistic analyses

The range of FoS per set of 1000 simulations for slopes of different inclined angle and CL is shown in Figure *17*. It demonstrates that the smaller the correlation length is the more concentrated the ranges of FoS are.

Two types of failure mechanisms were observed from the probabilistic analyses which are shown in Figure *18*. These were obtained by observing the weakest shear planes within the slope. Figure 19 shows the corresponding spatial distribution of the slopes associated with these failure mechanisms:

- For slope angles (e.g. 14.04°) under a value close to ϕ'_{mean} (in this instance 37°), the weakest shear planes are random and always occur along a plane with the lowest ϕ' spatial distribution. Thus, the failure mechanism varied when the CL was varied and was also different for each individual simulation (Figure *18*(a) and (b)).
- For slope angles (e.g. 46°) over a value close to ϕ'_{mean} (in this instance greater than 37°), the weakest shear planes always occur from the crest to the toe of the slope. This observation was consistent regardless of the CL (Figure *18*(c) and (d)).

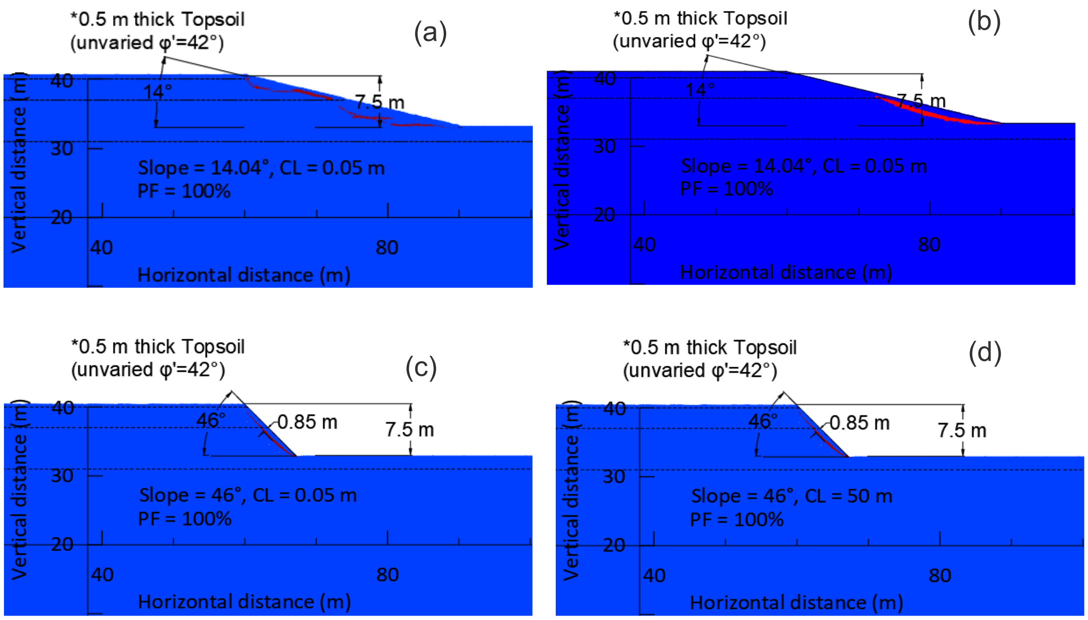

Figure 18 Failure mechanisms for slope angles:(a) Slope = 14.04 and CL = 0.05 m (b) Slope = 14.04° and CL = 50 m (c) Slope = 46 and CL = 0.05 m (d) Slope = 46° and CL = 50 m respectively.

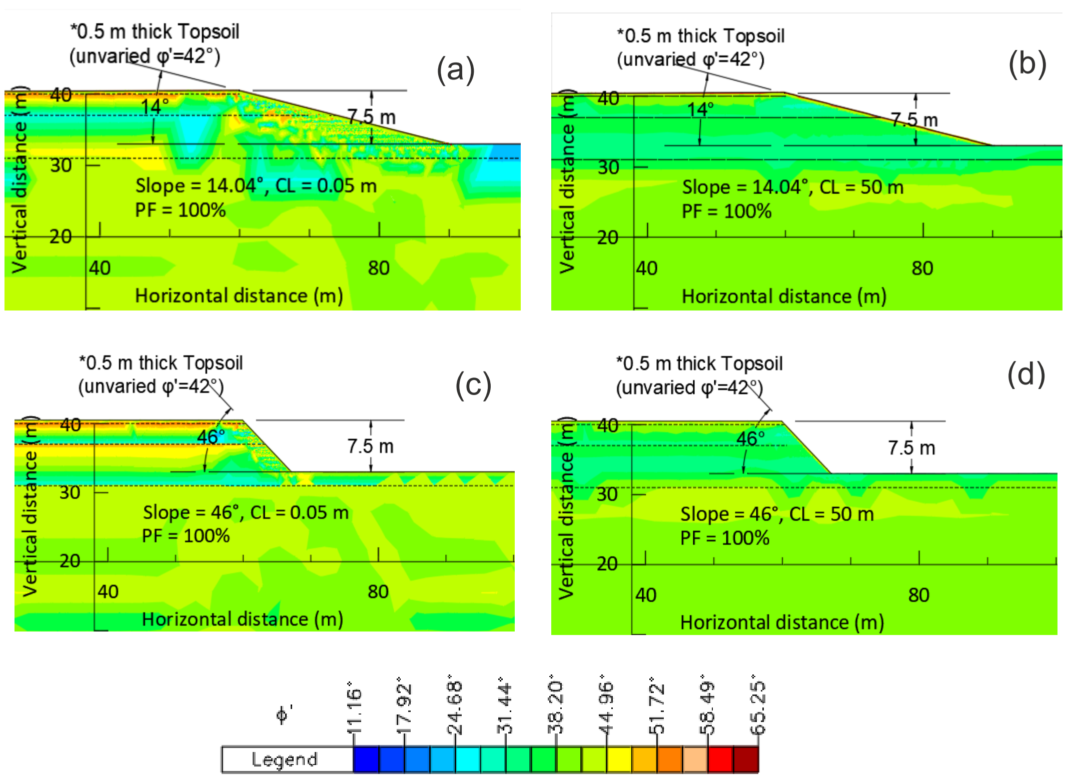

Figure 19 Corresponding spatial distribution of effective friction angles for the failure mechanisms of a slope: (a) slope angle = 14.04° and CL = 0.05 m, (b) slope angle = 14.04° and CL = 50 m, (c) slope angle = 46° and CL = 0.05 m, and (d) Slope = 46° and CL = 50 m.

As a sensitivity check, a set of probabilistic analyses were also carried out considering statistical zones (Option B). The results for these are shown in

Table *3*. Clearly, the trends for Option B coincide with those of Option A except that the slope angle at which an increase in the CL improves the design occurred at 37° for Option A but 34° for Option B. This difference is attributed to the fact that Zone I of Option had a standard deviation of 10.84° which is greater than the standard deviation of Option A (7.86°).

Table 3 Probability of Failure (%) for various slope angles and Correlation Lengths – Option B (considering layers). Probability of failure with grey background indicate the case that slope angle is less than ϕ'_{mean} and CL is within the calibrated range from CPT data. UB and LB represent results from upper bound and lower bound limit analyses, respectively.

CL \ **Slope angle (º)**	14.04	30	34	37	40	43	46
0.05 (UB)	0%	0%	1%	37%	85%	100%	100%
0.05 (LB)	0%	0%	0%	1%	29%	88%	100%
0.5 (UB)	0%	4%	14%	34%	55%	79%	93%
0.5 (LB)	0%	2%	9%	23%	46%	70%	88%
5 (UB)	0%	11%	22%	34%	48%	62%	75%
5 (LB)	0%	9%	19%	31%	44%	58%	71%
50 (UB)	0%	11%	22%	34%	47%	59%	71%
50 (LB)	0%	10%	20%	31%	44%	57%	69%

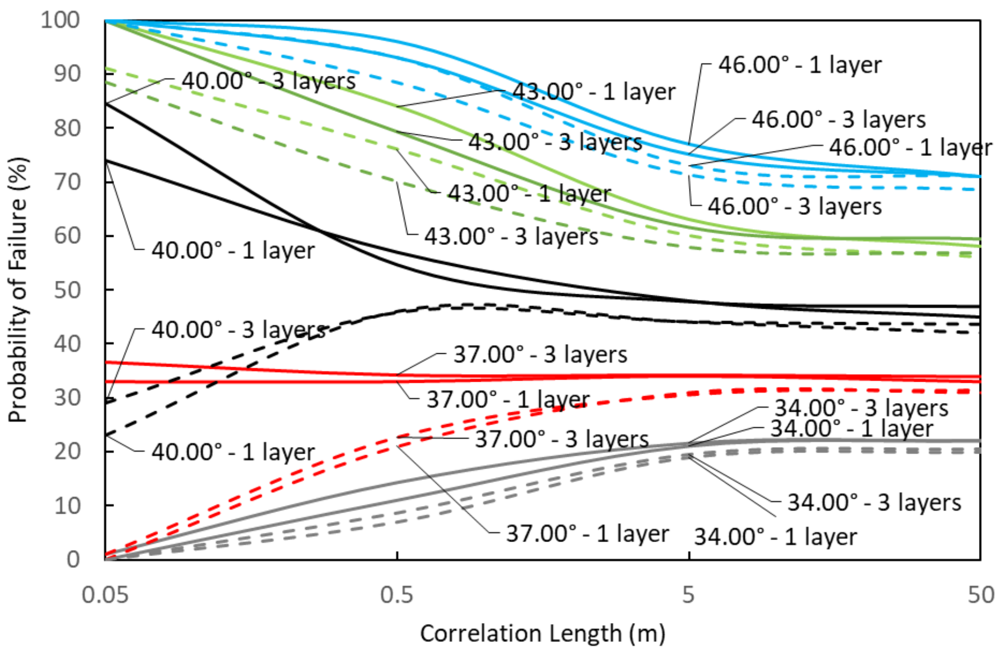

Figure 20 - Comparisons between Probabilistic analyses for layered vs non-layered analyses. Solid curves are from upper bound analysis whereas dash curves are from lower bound analysis.

Figure 20 illustrates the differences between solutions for Options A and B. Generally, the two solutions tend to converge when the CL is greater than 5 m. For slopes between a CL of 0.5 m and 5 m, a small difference in PF of 2% (max) was observed between the Option A and B. The maximum difference in PF for both analyses occurred at the lowest CL considered (0.05 m) for slopes between 37° and 43°. A maximum difference of 11% was observed at a slope of 40°. In addition, Figure *20* illustrates that for slopes between 37° and 43°, the smaller the CL, the larger the difference between the upper and lower bound limit solutions. The greatest difference occurred for a slope of 40° and a CL of 0.05m (51% for Option A and 56% for Option B). For the 40° slope and a CL of 50 m, the difference between the upper and lower bound solutions was 3% for both Option A and Option B.

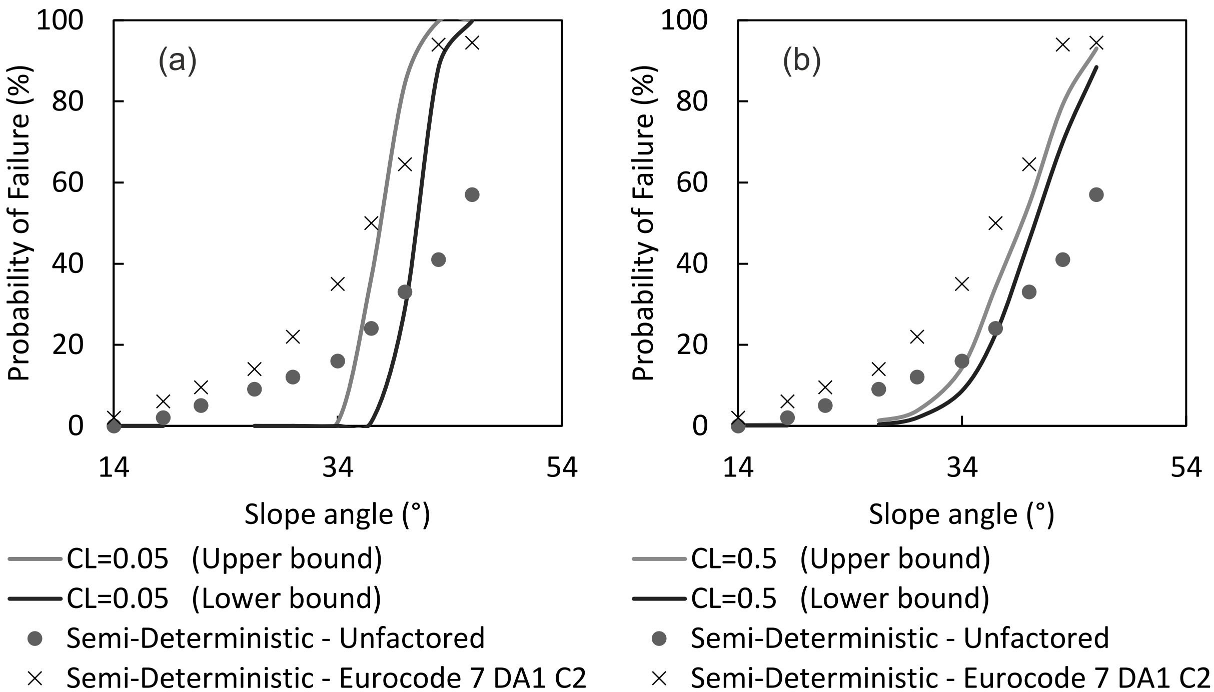

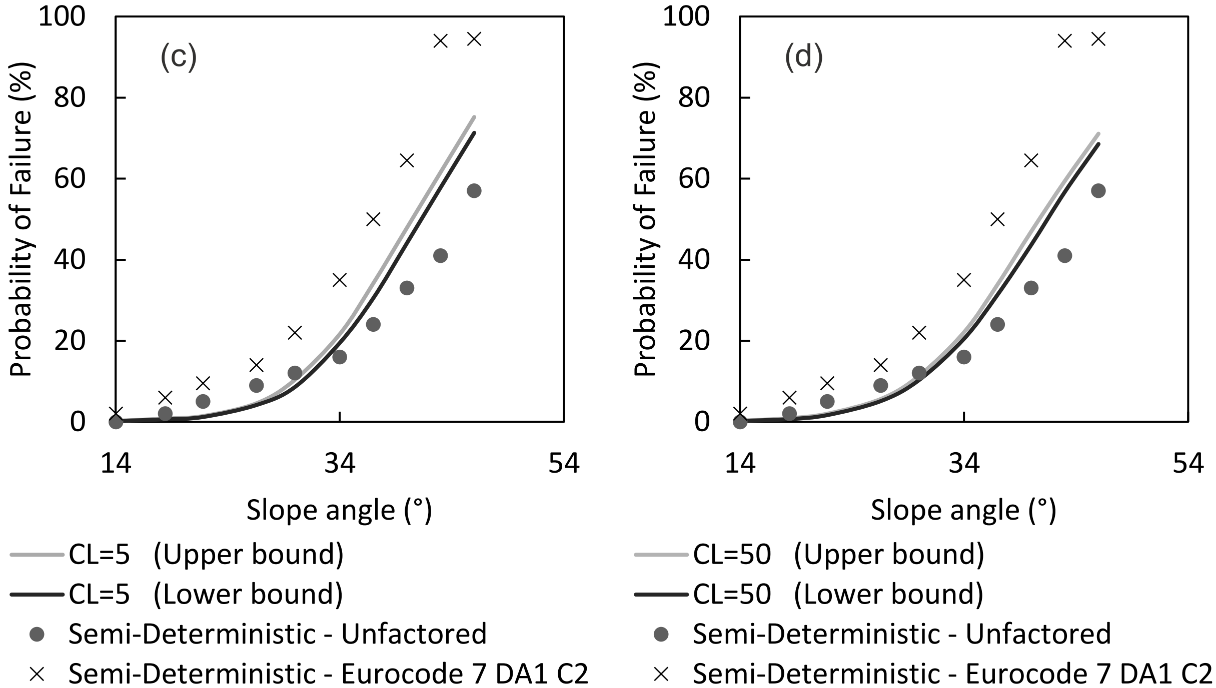

Figure 21 Semi-Deterministic vs Probabilistic analyses: (a) CL = 0.05 m vs semi-deterministic (b) CL = 0.5 m vs semi-deterministic (c) CL = 5 m vs semi-deterministic and (d) CL = 50m vs semi-deterministic

Figure 21 shows that the semi-deterministic analyses with unfactored effective frictional angle are more conservative than the probabilistic analyses as the slope angle becomes shallower but tends to be less conservative as the slope angle becomes steeper. Depending on the CL, there exists a slope angle below which the semi-deterministic analysis is always conservative meaning that it predicts a higher PF than the probabilistic analysis does.

Empirical design such as that of Ciria 185 (Nicholson, et al., 1999) suggests a semi-deterministic analysis based on a Factor of Safety using the most probable φ' (φ'$_{median}$) (≈40° from Figure 7*). Using the chart provided in*

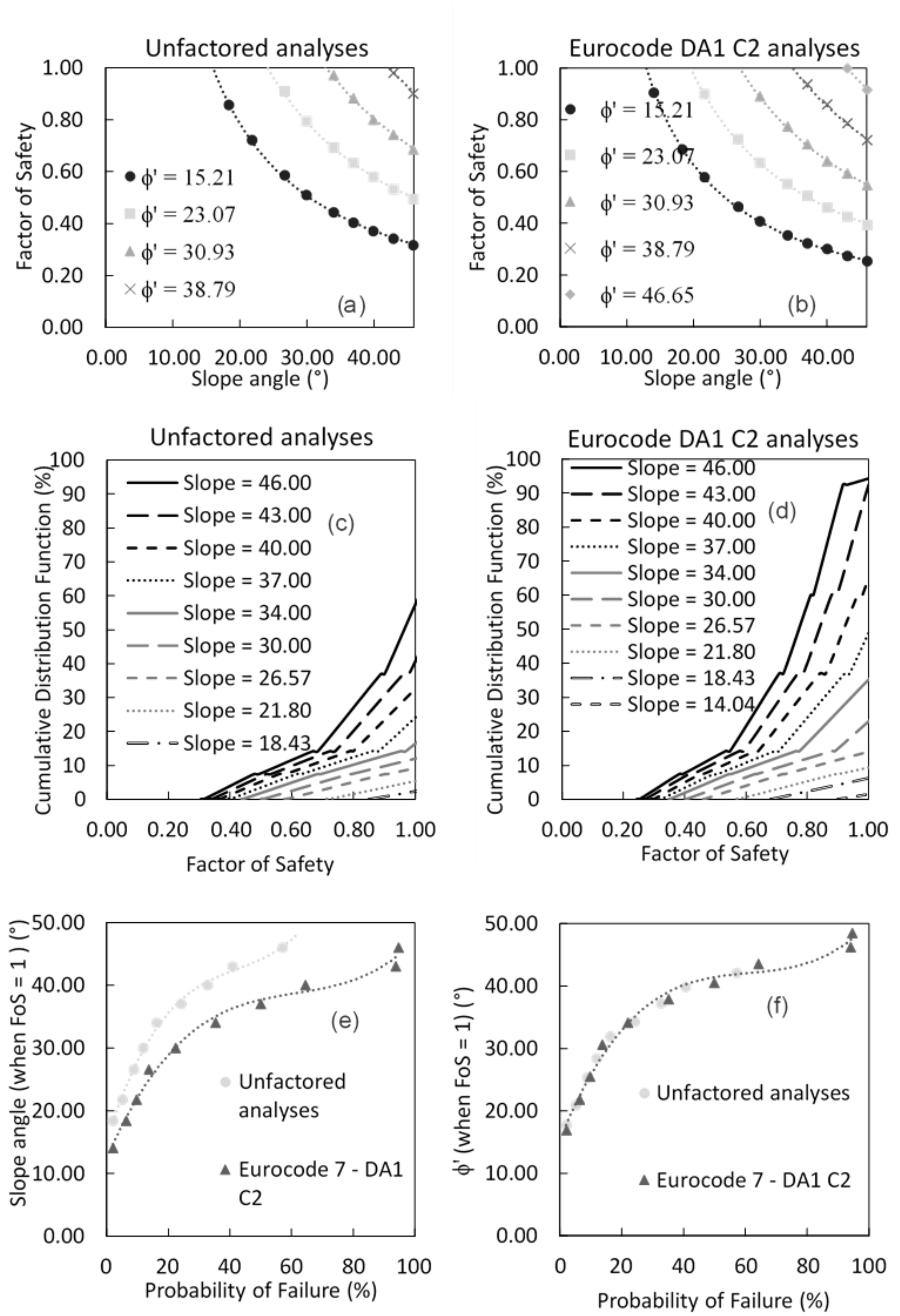

Figure 15, such an analysis would be stable for a slope of 43° or less for unfactored analyses and 37° or less for Eurocode 7 Combination 2 analyses. When examined on Figure *21*, it shows that an unfactored analyses with a slope of 43° always yields a less safe solution than the probabilistic analyses but applying the Eurocode 7 partial factor always yields a safer solution than the probabilistic analyses.

Selection of a ϕ'_{median} as per Ciria 185 (Nicholson, et al., 1999) with the application of a partial factor does provide a level of safety more conservative than a probabilistic analysis. However, it must be recognised that due to the inherent variability of the ground, there is a level of risk (a PF) that is inherent in the design of such a slope depending on the slope angle and the CL of the soil. The probabilistic analyses for the survey data and design assumptions shows that a slope of 37° (considered safe for ϕ'_{median} = 40° as per Ciria 185 and Eurocode 7) would have a PF of 34% to 37% whereas as shown in Figure *21*, based on probabilistic analyses, a 0% PF would occur at a slope of 34° for CL = 0.05m, just under 26° for CL = 0.5m (a slope at 26% has an upper bound PF of 1% and a lower bound PF of 0%) and just under 22° for a CL of 5 m (a slope at 22% has an upper bound PF of 1% and a lower bound PF of 1%).

7. Conclusions

This paper presents the investigation of the spatial variability of the effective friction angle of Crag deposits located in the east coast of England. Cone penetration test (up to 12 meters below ground level) was carried out at 26 locations to calibrate the spatial distribution characteristic of the effective friction angle. Additionally, both semi-deterministic (i.e. with unfactored strength or partial factored strength according to Eurocode 7) and full probabilistic analyses were carried out with finite element limit analysis method to study the slope stability in Crag deposit with eventual goal to help slope design in practice. Findings and conclusions from this study are summarised as follows.

(1) The statistical characteristic of effective friction angle of Crag deposit is disclosed which can be used as a reference when field data of crag deposit is not readily available. The Crag deposit up to 12 m below the ground level (bgl) can be approximately divided into three zones. The spatial variability of the effective friction angle obeys normal distribution. The top 3 m of the soil has a mean ($\mu_{\phi'}$) of $38.51°$ with a high standard deviation ($\sigma_{\phi'}$) of $10.84°$. The high standard deviation is most likely due to the present of organic content, and environmental, biological and human activities. The effective friction angle increases from 34.5° to 42° gradually with standard deviation decreasing steadily from 10° to $6.53°$ from 3m (bgl) to 9 m (bgl). At depths greater than 9 m up to 12 m bgl, $\mu_{\phi'}$ gradually increased to $41.60°$ but the standard deviation was now only $1.84°$ (over 5 times less than the standard deviation in the top 3 m bgl). These findings imply that Crag's variability depends on depth, especially for the top 9 m bgl which for typical geotechnical designs is significant. Except for large earthworks where the top 9 m would be excavated, most geotechnical designs would be affected by this zone of variability.

(2) The nature of in-situ conditions (e.g. inclusion of organic content and oscillation of pore water pressures) have a significant influence on the estimation of vertical correlation length. The change from Crag deposit to organic soil leads to small spikes in the decay of autocovariance function while the oscillation of pore water pressure leads to frequent large spikes. The method of moments combined with Bayesian analysis can be used to consider these effects and uncertainties.

(3) The influence of the CL on the PF depends on the slope angle. When the slope angle is less than a value just under ϕ'_{mean}, a lower CL improves slope design. In contrast, when the slope angle is greater than a value just over ϕ'_{mean}, a higher CL improves slope design. Nevertheless, there

tends to be a limit beyond which an increase in the CL does not result in a significant change in the PF.

(4) The comparison between the semi-deterministic and probabilistic analyses shows that the application of a partial factor to ϕ'_{median} as recommended in Eurocode 7 and Ciria 185 (Nicholson, et al., 1999) does provide a safer solution than the unfactored and probabilistic analyses. However, it was shown that use of a semi-deterministic parameter such as ϕ'_{median} (even with the application of a partial factor) still has an inherent but small risk present due to spatial variability of the soil. The decision on the value of PF considered acceptable depends on the impact of a slope stability failure, for example if the impact is minimal enough to be remediated through economic regular maintenance activities. Combinations of further analyses on the failure patterns and the cost of remediation or maintenance of slopes may help risk management of projects.

APPENDIX

All CPT profiles are given in this appendix for reuse.

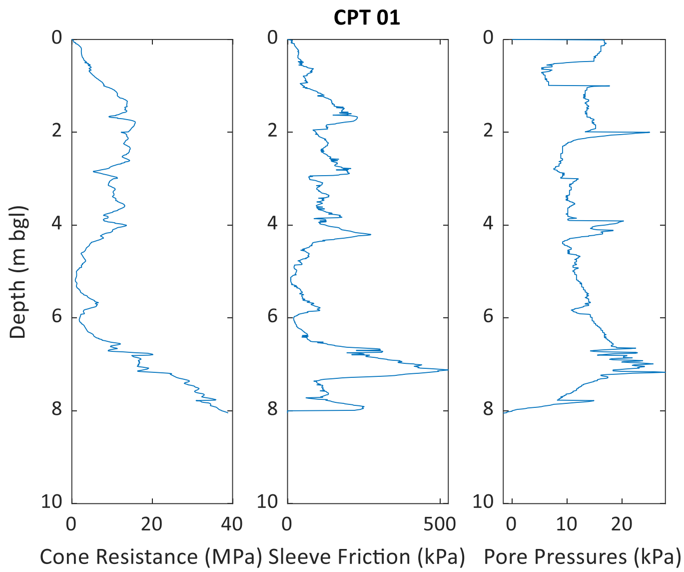

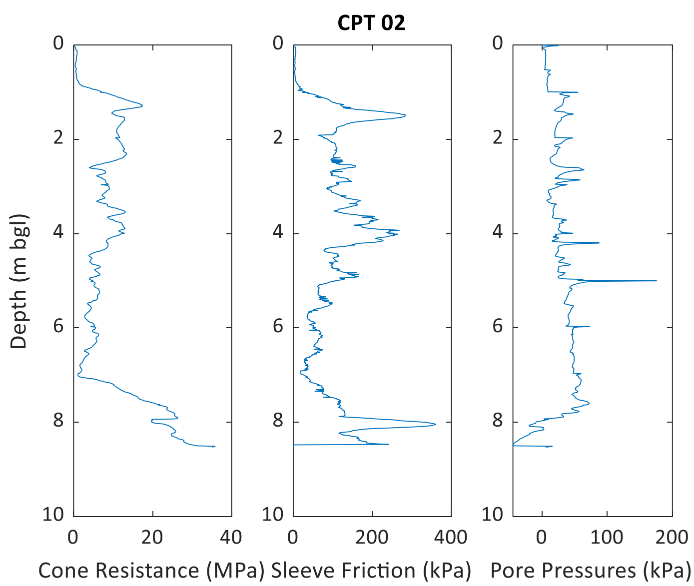

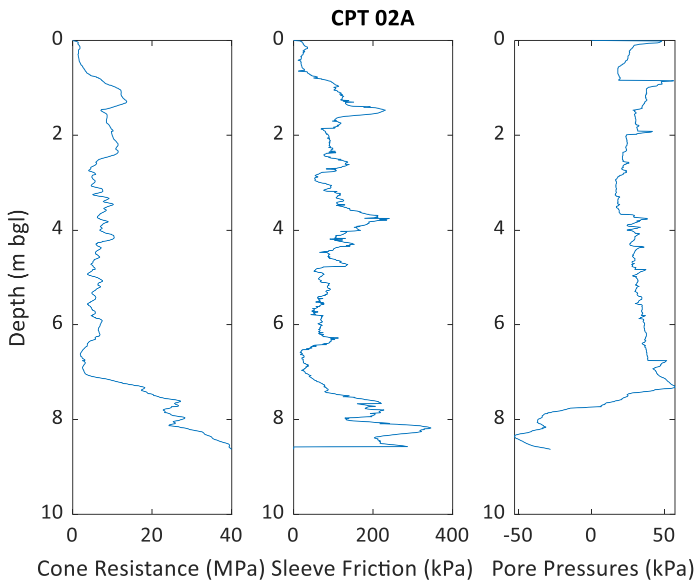
CPT 02A
Depth (m bgl)
Cone Resistance (MPa)
Sleeve Friction (kPa)
Pore Pressures (kPa)

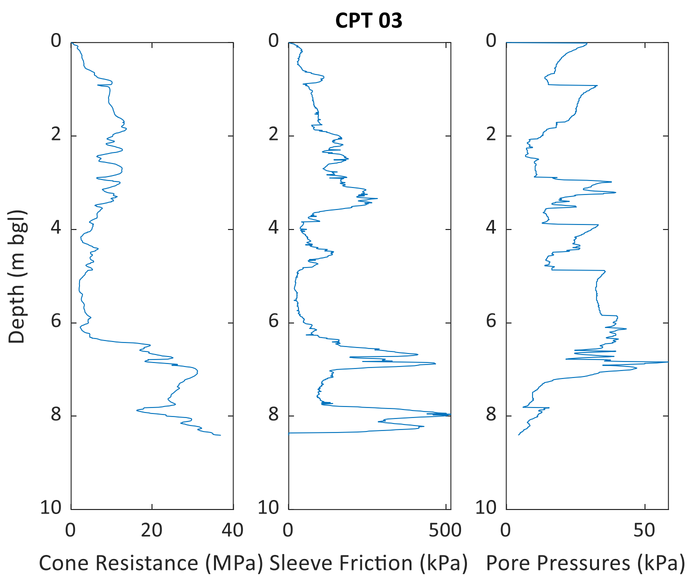
CPT 03
Depth (m bgl)
Cone Resistance (MPa)
Sleeve Friction (kPa)
Pore Pressures (kPa)

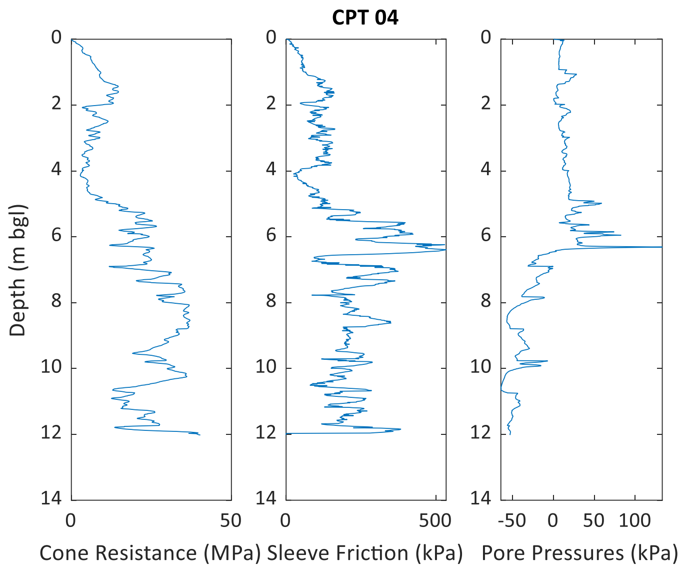
CPT 04
Depth (m bgl)
Cone Resistance (MPa)
Sleeve Friction (kPa)
Pore Pressures (kPa)

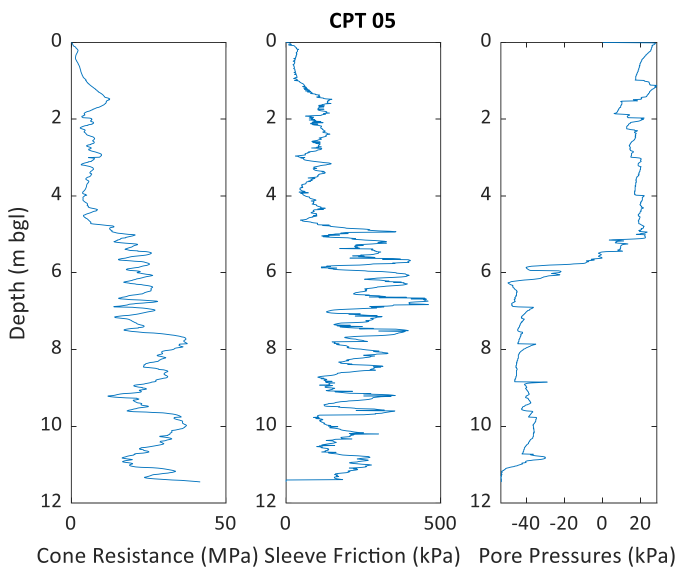
CPT 05
Depth (m bgl)
Cone Resistance (MPa)
Sleeve Friction (kPa)
Pore Pressures (kPa)

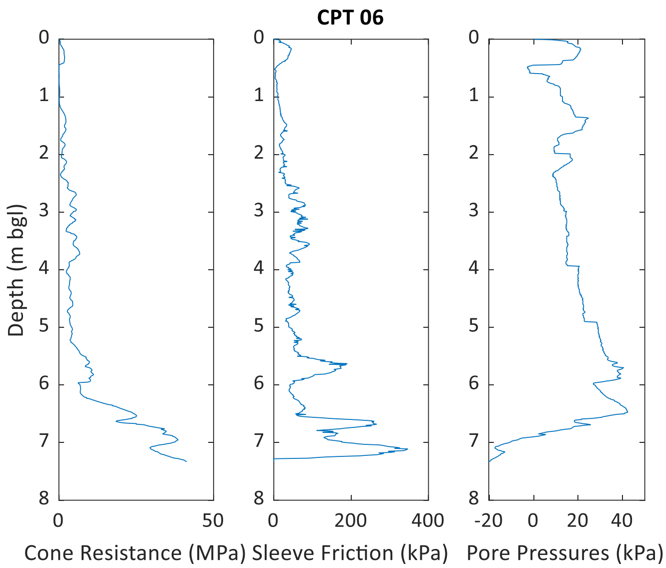
CPT 06
Depth (m bgl)
0
1
2
3
4
5
6
7
8
0
50
Cone Resistance (MPa)
0
200
400
Sleeve Friction (kPa)
-20
0
20
40
Pore Pressures (kPa)

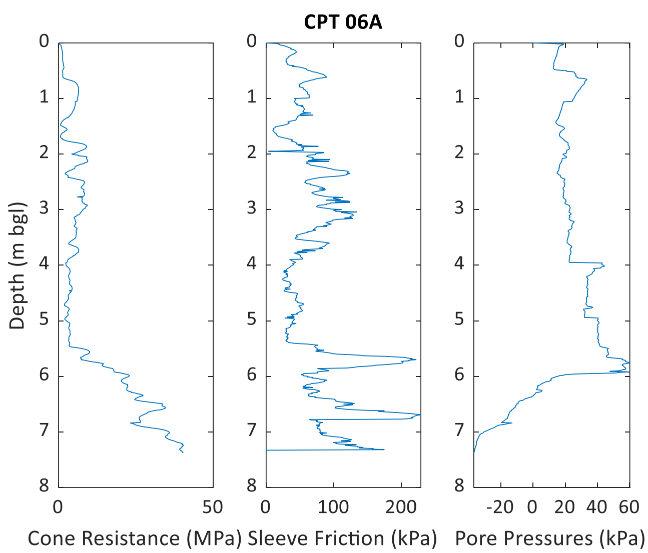
CPT 06A
Depth (m bgl)
0
1
2
3
4
5
6
7
8
0
50
Cone Resistance (MPa)
0
100
200
Sleeve Friction (kPa)
-20
0
20
40
60
Pore Pressures (kPa)

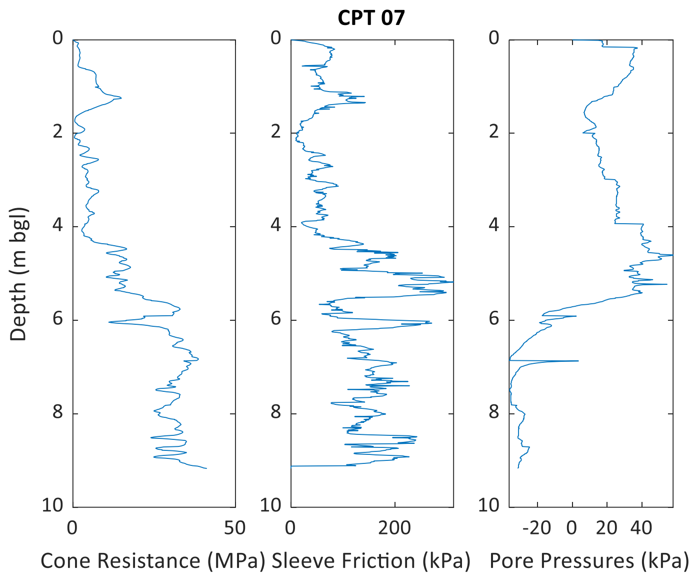
CPT 07
Depth (m bgl)
0
2
4
6
8
10
0
50
200
-20 0 20 40
Cone Resistance (MPa) Sleeve Friction (kPa) Pore Pressures (kPa)

647

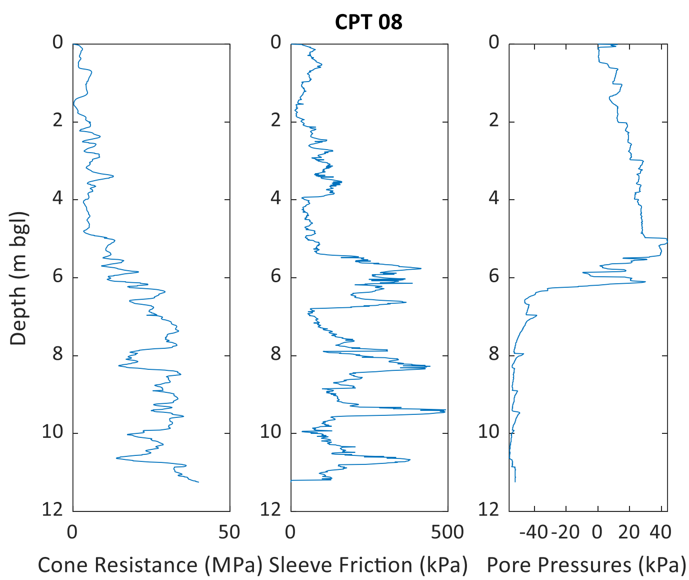
CPT 08
Depth (m bgl)
0
2
4
6
8
10
12
0
50
500
-40 -20 0 20 40
Cone Resistance (MPa) Sleeve Friction (kPa) Pore Pressures (kPa)

648

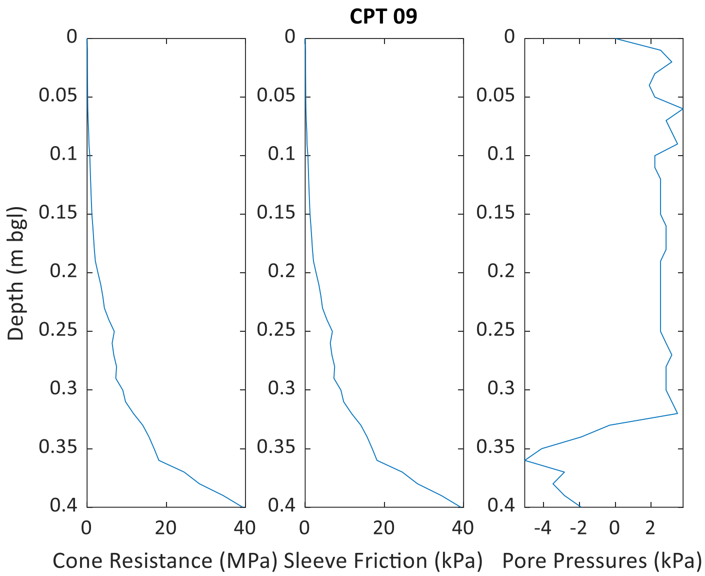
CPT 09
Depth (m bgl)
Cone Resistance (MPa)
Sleeve Friction (kPa)
Pore Pressures (kPa)

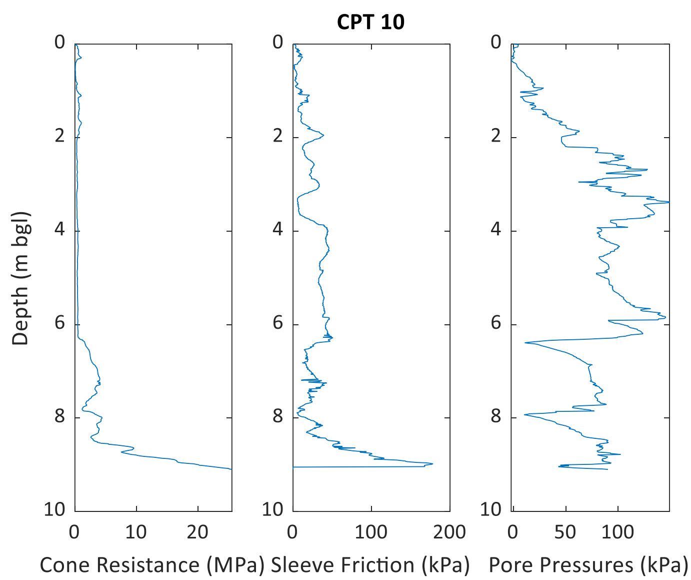
CPT 10
Depth (m bgl)
Cone Resistance (MPa)
Sleeve Friction (kPa)
Pore Pressures (kPa)

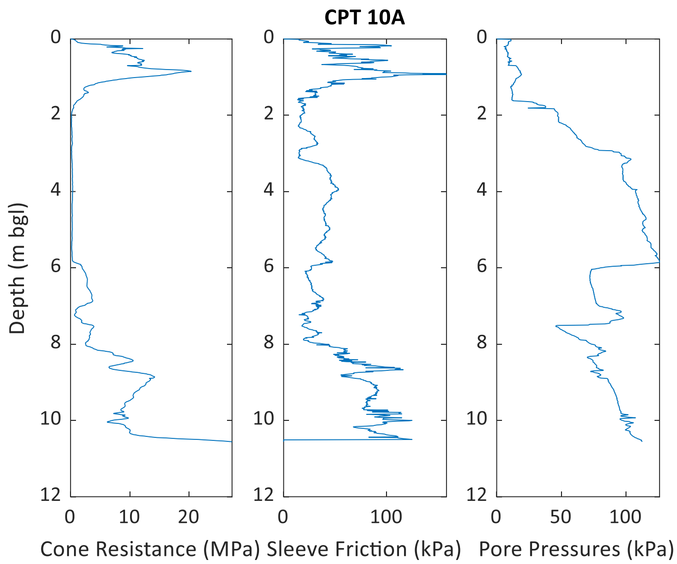
CPT 10A
Depth (m bgl)
0
2
4
6
8
10
12
0 10 20
Cone Resistance (MPa)
0 100
Sleeve Friction (kPa)
0 50 100
Pore Pressures (kPa)

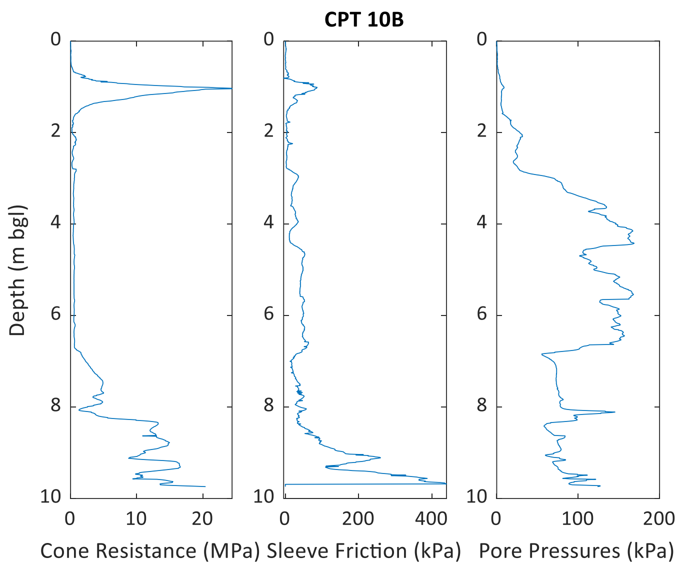
CPT 10B
Depth (m bgl)
0
2
4
6
8
10
0 10 20
Cone Resistance (MPa)
0 200 400
Sleeve Friction (kPa)
0 100 200
Pore Pressures (kPa)

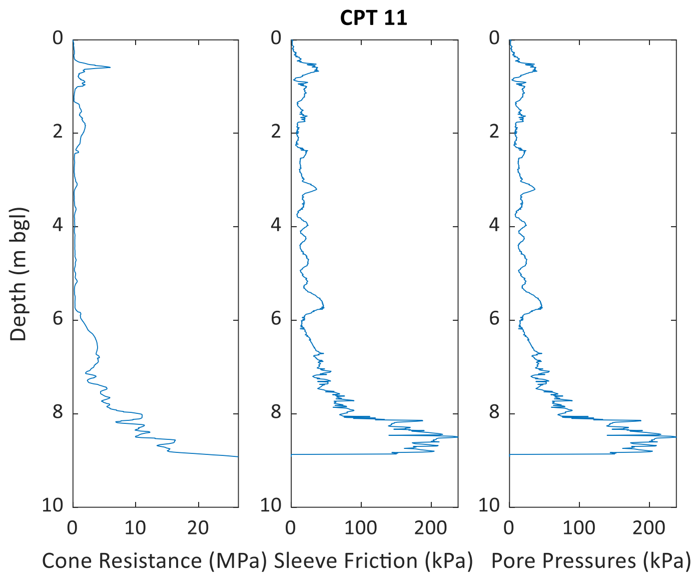
CPT 11
Depth (m bgl)
Cone Resistance (MPa)
Sleeve Friction (kPa)
Pore Pressures (kPa)

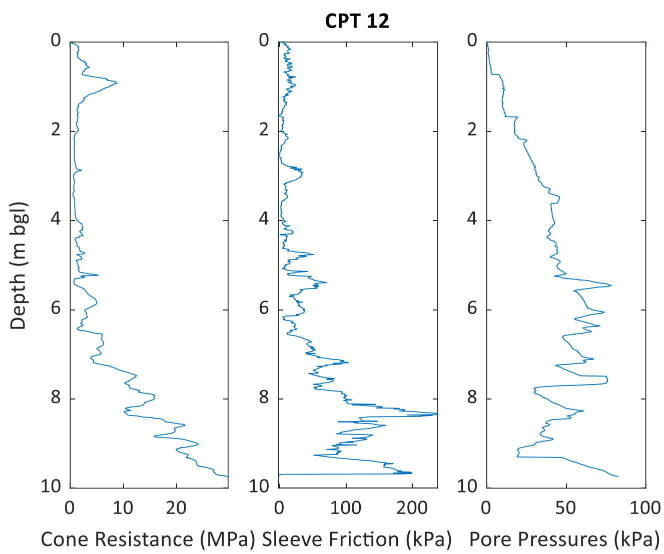
CPT 12
Depth (m bgl)
Cone Resistance (MPa)
Sleeve Friction (kPa)
Pore Pressures (kPa)

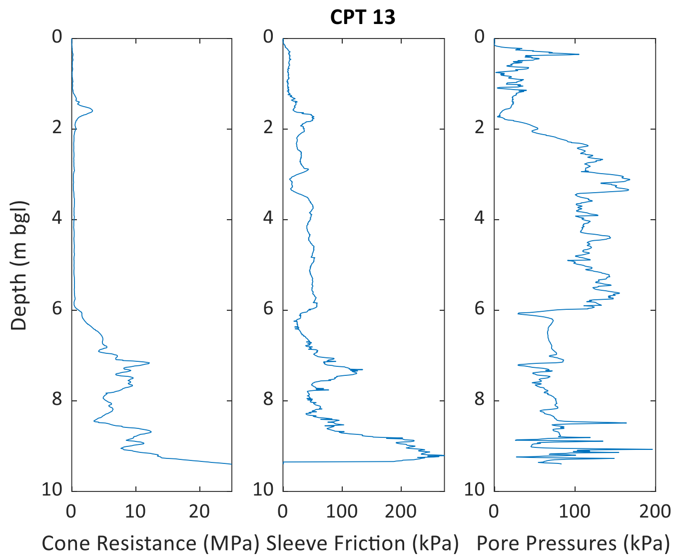
CPT 13
Depth (m bgl)
Cone Resistance (MPa)
Sleeve Friction (kPa)
Pore Pressures (kPa)

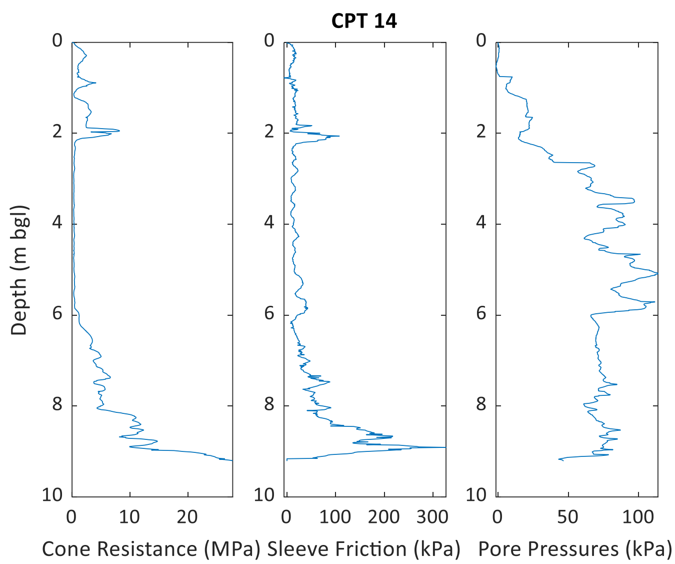
CPT 14
Depth (m bgl)
Cone Resistance (MPa)
Sleeve Friction (kPa)
Pore Pressures (kPa)

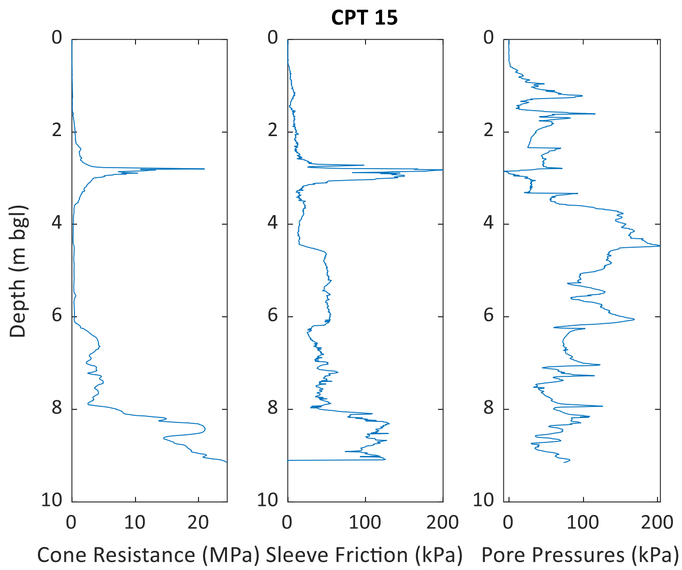
CPT 15
Depth (m bgl)
Cone Resistance (MPa)
Sleeve Friction (kPa)
Pore Pressures (kPa)

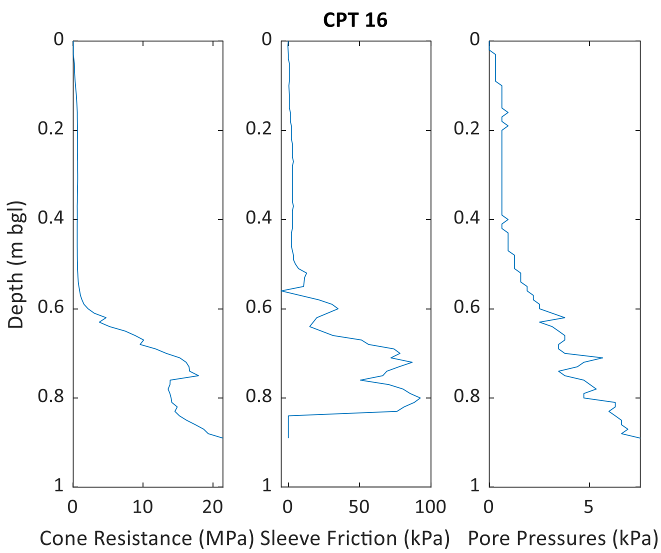
CPT 16
Depth (m bgl)
Cone Resistance (MPa)
Sleeve Friction (kPa)
Pore Pressures (kPa)

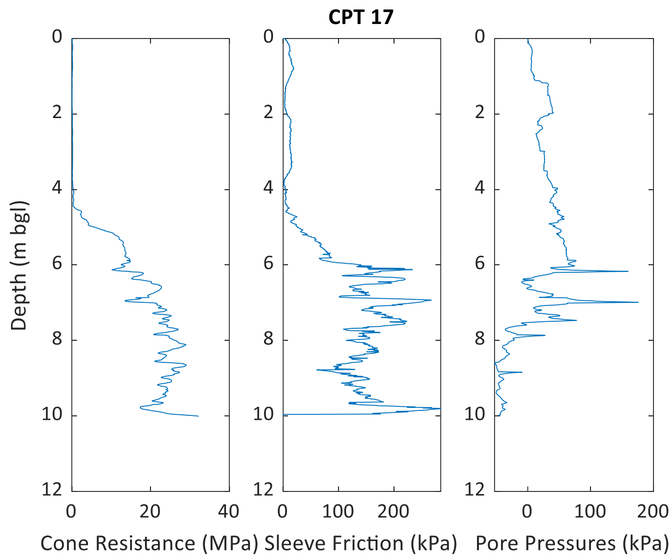
CPT 17
Depth (m bgl)
0
2
4
6
8
10
12
0
20
40
100
200
Cone Resistance (MPa) Sleeve Friction (kPa) Pore Pressures (kPa)

659

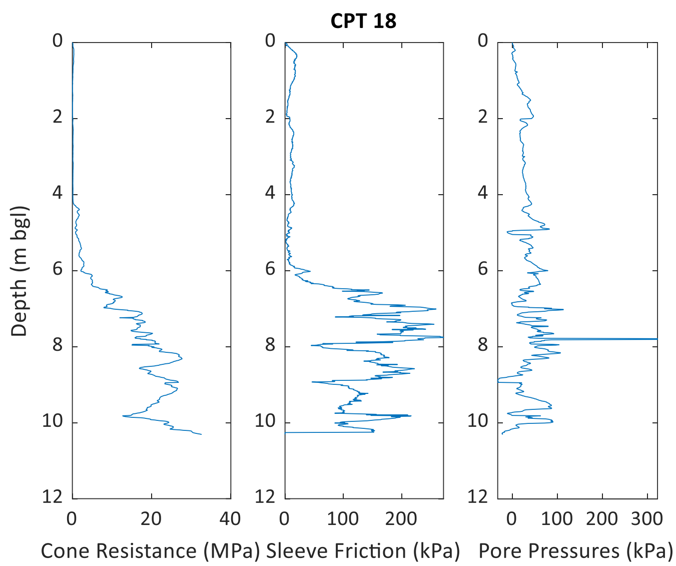
CPT 18
Depth (m bgl)
0
2
4
6
8
10
12
0
20
40
100
200
300
Cone Resistance (MPa) Sleeve Friction (kPa) Pore Pressures (kPa)

660

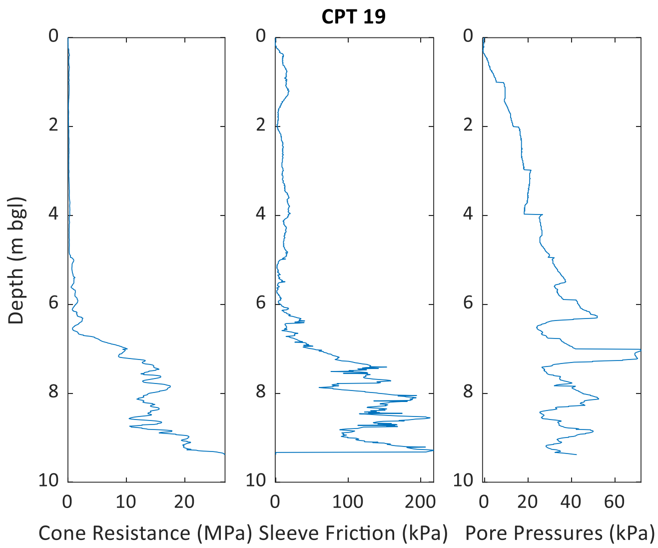
CPT 19
Depth (m bgl)
Cone Resistance (MPa)
Sleeve Friction (kPa)
Pore Pressures (kPa)

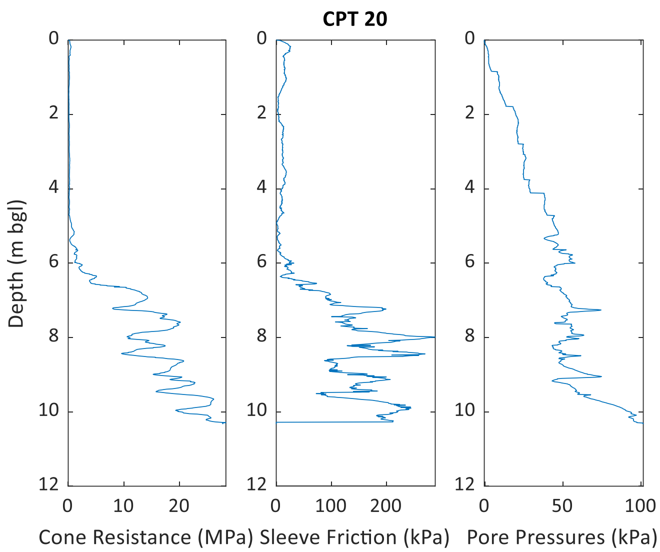
CPT 20
Depth (m bgl)
Cone Resistance (MPa)
Sleeve Friction (kPa)
Pore Pressures (kPa)

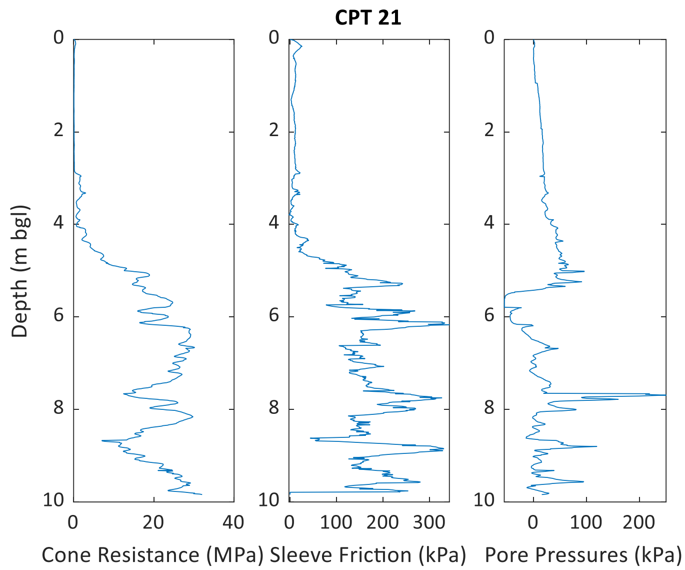

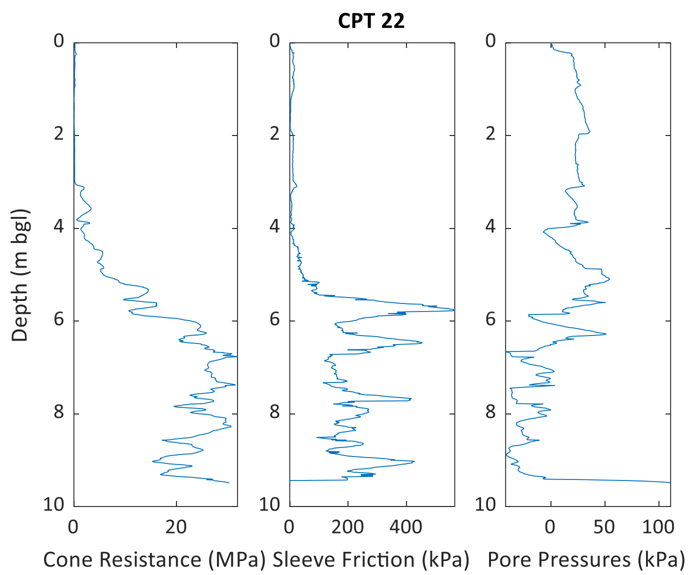

ACKNOWLEDGEMENTS

The second author appreciates the financial support given by UK EPSRC New Investigator Award project (EP/V012169/1).

References

Abrahamsen, P., 1997. *A review of Gaussian Random Fields and Correlation Functions.* 2nd ed. Oslo: Norwegian Computing Center.

Ali, A. et al., 2017. Probabilistic stability assessment using adaptive limit analysis and random fields. *Acta Geotechnica,* Volume 12, pp. 937-948.

Andrieu, C. & Thoms, J., 2008. A tutorial on adaptive MCMC. *Statistics and Computing,* Volume 18, pp. 343-373.

Baker, R. & Garber, M., 1978. Theoretical analysis of the stability of slopes. *Geotechnique,* 28(4), pp. 395-411.

Beck, J. L. & Au, S.-K., 2002. Bayesian updating of structural models and reliability using Markov Chain Monte Carlo simulation. *Journal of Engineering Mechanics (ASCE),* 128(4), pp. 380-391.

British Geological Survey, 1996. *Sheet 176 - Lowestoft - Solid and Drift,* United Kingdom: British Geological Survey.

British Geological Survey, 2021. *Geology of Britain Viewer.* [Online] Available at: https://mapapps.bgs.ac.uk/geologyofbritain/home.html [Accessed 22 January 2021].

British Standards International (BSI), 2004 + A1:2013. *Eurocode 7: Geotechnical design - Part 1: General Rules (BS EN 1997-1:2004 + A1:2013).* s.l.:British Standards Limited.

British Standards International (BSI), 2007. *BS EN 1997-2:2007 - Eurocode 7 - Part 2: Ground investigation and testing.* s.l.:British Standards International (BSI).

British Standards International (BSI), 2015. *BS 8002:2015.* s.l.:British Standards International (BSI).

Cami, B., Javankhoshdel, S., Phoon, K.-K. & Ching, J., 2020. Scale of fluctuation for spatially varying soils: estimation methods and values. *American Society of Civil Engineers (ASCE) Journal of Risk and Uncertainty in Engineering Systems, Part A: Civil Engineering,* 6(4), pp. 03120002-1 to 16.

Cao, Z. & Wang, Y., 2013. Bayesian approach for probabilistic site characterization using Cone Penetration Tests. *American Society of Civil Engineers (ASCE) Journal of Geotechnical and Geoenvironmental Engineering,* 139(2), pp. 267-276.

Ching, J. & Phoon, K.-K., 2019. Constructing site-specific multivariate probability distribution model using Bayesian Machine Learning. *American Society of Civil Engineers (ASCE) Journal of Engineering Mechanics,* 145(1), pp. 04018126-1 to 15.

Ching, J., Wu, S. & Phoon, K.-K., 2021. Constructing quasi-site-specific multivariate probability distribution using hierachical Bayesian Model.. *American Society of Civil Engineers (ASCE) Journal of Engineering Mechanics,* 147(10), pp. 04021069-1 to 18.

Ching, J., Wu, T.-J., Stuedlein, A. W. & Bong, T., 2018. Estimating horizontal scale of fluctuation with limited CPT soundings. *Geoscience Frontiers,* Volume 9, pp. 1597-1608.

De Groot, D. J. & Baecher, G. B., 1993. Estimating autocovariance of in-situ soil properties. *ASCE Journal of Geotechnical Engineering,* 119(1), pp. 147-167.

Drucker, D. C. & Prager, W., 1952. Soil Mechanics and Plastic analysis or Limit design. *Quarterly of Applied Mathematics,* 10(2), pp. 157-165.

Dyson, A. P. & Tolooiyan, A., 2019. Prediction and classification for finite element slope stability analysis by random field comparison. *Computers and Geotechnics*, 109, pp. 117-129.

El-Ramly, H., Morgenstern, N. R. & Cruden, D. M., 2002. Probabilistic slope stability analysis for practice. *Canadian Geotechnical Journal,* 39(3), pp. 665-683.

Fenton, G. A. & Griffiths, D. V., 2008. *Risk Assessment in Geotechnical Engineering.* First Edition ed. New Jersey: John Wiley and Sons.

Goodman, J. & Weare, J., 2010. Ensemble samplers with affine invariance. *Communications in Applied Mathematics and Computational Science,* Volume 5, pp. 65-80.

Griffiths, D. V. & Fenton, G. A., 2004. Probabilistic Slope Stability Analysis by Finite Elements. *Journal of Geotechnical and Geoenvironmental Engineering,* 130(5), pp. 507-518.

Griffiths, D. V., Huang, J. & Fenton, G. A., 2009. Influence of spatial variability on slope reliability using 2D random fields. *American Society of Civil Engineers (ASCE) Journal of Geotechnical and Geoenvironmental Engineering,* 135(10), pp. 1367-1378.

Griffiths, D. V. & Lane, P. A., 1999. Slope stability analysis by finite elements. *Geotechnique,* 49(3), pp. 387-403.

Huang, J., Griffiths, D. V. & Fenton, G. A., 2010. System reliability of slopes by RFEM. *Japanese Geotechnical Society,* 50(3), pp. 343-353.

Huang, J. et al., 2013. Quantitative risk assessment of landslide by limit analysis and random fields. *Computers and Geotechnics,* Volume 53, pp. 60-67.

Jiang, S.-H. & Huang, J.-S., 2016. Efficient slope reliability analysis at low-probability levels in spatially variable soils. *Computers and Geotechnics,* Volume 75, pp. 18-27.

Jiang, S.-H.et al., 2015. Efficient system reliability analysis of slope stability in spatially variable soils using Monte Carlo simulation. *American Society of Civil Engineers (ASCE), Journal of Geotechnical and Geoenvironmental Engineering,* 141(2), pp. 04014096-1 to 13.

Jiang, S.-H., Li, D.-Q., Zhang, L.-M. & Zhou, C.-B., 2014. Slope reliability analysis considering spatially variable shear strength parameters using a non-intrusive stochastic finite element method. *Engineering Geology,* Volume 168, pp. 120-128.

Krabbenhoft, K., Huang, J. & Optum Computational Engineering, 2018. *Optum G2: Theory.* s.l.:Optum Computational Engineering.

Kulhawy, F. H. & Mayne, P. W., 1990. *Manual on estimating soil properties for foundation design,* New York: Cornell University.

Lacasse, S. & Nadim, F., 1996. Uncertainties in Characterising Soil Properties. *ASCE - Geotechnical Special Publication No. 58 - Uncertainty in the geologic Environment: From Theory to Practice,* Volume 1, pp. 49-75.

Liang, T., Knappett, J. A. & Duckett, N., 2015. Modelling the seismic performance of rooted slopes from individual root-soil interaction to global slope behaviour. *Geotechnique,* 65(12), pp. 995-1009.

Li, D.-Q., Xiao, T., Phoon, K.-K. & Zhou, C.-B., 2016. Efficient and consistent reliability analysis of soil slope stability using both limit equilibrium analysis and finite element analysis. *Applied Mathematical Modelling,* Volume 40, pp. 5216-5229.

Liu, X., Li, D.-Q., Cao, Z.-J. & Wang, Y., 2020. Adaptive Monte Carlo simulation method for system reliability analysis of slope stability based on limit equilibrium methods. *Engineering Geology,* Volume 264.

Low, B. K., 2019. Probabilisitic insights on a soil slope in San Francisco and a rock slope in Hong Kong. *Georisk,* 13(4), pp. 326-332.

Lye, A., Cicirello, A. & Patelli, E., 2021a. Sampling methods for solving Bayesian model updating problems: A tutorial. *Mechanical Systems and Signal Processing,* Volume 159, p. 107760.

Lye, A., Cicirello, A. & Patelli, E., 2021b. An efficient and robust sampler for Bayesian inference: Transitional Ensemble Markov Chain Monte Carlo. *Mechanical Systems and Signal Processing,* pp. (Accepted 20th September, 2021).

Malekpoor, S. P., Jamshidi, C. & Javankhoshdel, S., 2020. Discussion of "Probabilistic seismic slope stability analysis and design. *Canadian Geotech Journal,* 56(12), pp. 1979-1998.

Melchers, R. E., 1987. *Structural Reliability Analysis & Prediction.* New York: Wiley.

Morgenstern, N. R. & Price, V. E., 1965. The Analysis of the stability of general slip surfaces. *Géotechnique,* 15(1), pp. 79-93.

Nicholson, D., Tse, C.-M. & Penny, C., 1999. *CIRIA Report 185 - The Observational Method in ground engineering: principles and applications,* Dorset: Ciria.

Phoon, K. K., Huang, S. P. & Quek, S. T., 2002. Implementation of Karhunen-Loeve expansion for simulation using wavelet-Galerkin scheme. *Probabilistic Engineering Mechanics,* Volume 17, pp. 293-303.

Phoon, K.-K. & Kulhawy, F. H., 1999. Characterization of geotechnical variability. *Canadian Geotechnical Journal,* 36(4), pp. 612-624.

Prestwich, J., 1871. On the structure of the Crag-beds of Suffolk and Norfolk, with some observations on their organic remains. Part 1 - The Coralline Crag of Suffolk. *Journal of the Geological Society,* Volume 27, pp. 115-146.

Robertson, P. K., 2010. *Soil Behaviour Type from the CPT: an update.* California USA: Robertson, P K;.

Robertson, P. K. & Campanella, R. G., 1983. Interpretation of Cone Penetration Tests. *Canadian Geotechnical Journal,* 20(4).

Uzielli, M. & Mayne, P. W., 2019. Probabilistic assignment of effective friction angles of sands and silty sands from CPT using quantile regression. *Georisk: Assessment and Management of Risk for Engineered Systems and Geohazards.*

Vanmarke, E., 1983. *Random fields, analysis and synthesis.* 1st Edition ed. s.l.:The Massachusetts Institute of Technology.

Venturini, T. et al., 2016. Mapping slope deposits depth by means of cluster analysis: a comparative assessment. *Societa Geologica Italiana,* Volume 39, pp. 47-50.

Zalasiewicz, J. A. et al., 1988. Stratigraphy and Palaeoenvironments of the Red Crag and Norwich Crag Formations between Aldeburgh and Sizewell, Suffolk, England. *Philosophical Transactions of the Royal Society of London,* 322(1210), pp. 221-272.

Zheng, Z. & Dai, H., 2017. Simulation of multi-dimensional random fields by Karhunen-Loeve expansion. *Computational Methods: Applied Mechanical Engineering,* pp. 221-247.